AGU PUBLICATIONS

Paleoceanography

RESEARCH ARTICLE
10.1002/2016PA003056

Key Points:
- Frequent and systematic reductions in glacial admixture of northern sourced water masses to the Southern Ocean after 1.5 Ma
- Minimum Northern Component Water export to the Southern Ocean during the Intensification of North Hemispheric Glaciation
- Long-term changes from South American toward South African weathering inputs into the Southern Ocean documented by Hf isotopes

Supporting Information:
- Supporting Information S1

Correspondence to:
V. Dausmann,
vdausmann@geomar.de

Citation:
Dausmann, V., M. Frank, M. Gutjahr, and J. Rickli (2017), Glacial reduction of AMOC strength and long-term transition in weathering inputs into the Southern Ocean since the mid-Miocene: Evidence from radiogenic Nd and Hf isotopes, *Paleoceanography*, *32*, 265–283, doi:10.1002/2016PA003056.

Received 17 NOV 2016
Accepted 2 MAR 2017
Accepted article online 6 MAR 2017
Published online 20 MAR 2017

Glacial reduction of AMOC strength and long-term transition in weathering inputs into the Southern Ocean since the mid-Miocene: Evidence from radiogenic Nd and Hf isotopes

Veit Dausmann[1], Martin Frank[1], Marcus Gutjahr[1], and Jörg Rickli[2]

[1]GEOMAR Helmholtz-Centre for Ocean Research Kiel, Kiel, Germany, [2]Department of Earth Sciences, Institute of Geochemistry and Petrology, ETH Zurich, Zurich, Switzerland

Abstract Combined seawater radiogenic hafnium (Hf) and neodymium (Nd) isotope compositions were extracted from bulk sediment leachates and foraminifera of Site 1088, Ocean Drilling Program Leg 177, 2082 m water depth on the Agulhas Ridge. The new data provide a continuous reconstruction of long- and short-term changes in ocean circulation and continental weathering inputs since the mid-Miocene. Due to its intermediate water depth, the sediments of this core sensitively recorded changes in admixture of North Atlantic Deep Water to the Antarctic Circumpolar Current as a function of the strength of the Atlantic Meridional Overturning Circulation (AMOC). Nd isotope compositions (ε_{Nd}) range from −7 to −11 with glacial values generally 1 to 3 units more radiogenic than during the interglacials of the Quaternary. The data reveal episodes of significantly increased AMOC strength during late Miocene and Pliocene warm periods, whereas peak radiogenic ε_{Nd} values mark a strongly diminished AMOC during the major intensification of Northern Hemisphere Glaciation near 2.8 Ma and in the Pleistocene after 1.5 Ma. In contrast, the Hf isotope compositions (ε_{Hf}) show an essentially continuous evolution from highly radiogenic values of up to +11 during the Miocene to less radiogenic present-day values (+2 to +4) during the late Quaternary. The data document a long-term transition in dominant weathering inputs, where inputs from South America are replaced by those from Southern Africa. Moreover, radiogenic peaks provide evidence for the supply of radiogenic Hf originating from Patagonian rocks to the Atlantic sector of the Southern Ocean via dust inputs.

1. Introduction

It has been demonstrated by numerous studies that global climate has been closely linked to the strength of the meridional overturning circulation in the Atlantic Ocean (AMOC) [e.g., *Broecker et al.*, 1985; *Enfield et al.*, 2001; *Sutton and Hodson*, 2005]. In this context it is important to understand the processes governing present and past changes in the strength and flow paths of the water masses of the AMOC. Variations of AMOC strength have been monitored directly during the last decade and have been attributed to adjustments of water mass density in the Labrador Sea due to changes in temperature and salinity in the North Atlantic [e.g., *Robson et al.*, 2015; *Jackson et al.*, 2016]. Furthermore, variations in the net heat transfer from the Southern Hemisphere to the Northern Hemisphere via the Agulhas Leakage are thought to contribute to fluctuations in AMOC strength [*Biastoch et al.*, 2008]. The export of heat and salt from the Southern Ocean (SO) and Indian Ocean regulates chemical and physical properties of water masses in the Atlantic, especially in the formation region of the North Atlantic Deep Water (NADW) [*Gordon et al.*, 1992].

There is general consensus that millennial-scale and glacial-interglacial (G-I) climate oscillations have been linked to a seesaw between a "warm" mode and a "cold" mode of NADW export to the Southern Ocean and thus AMOC strength [e.g., *Boyle and Keigwin*, 1982; *Curry and Lohmann*, 1982; *Oppo and Fairbanks*, 1987; *Rutberg et al.*, 2000; *Piotrowski*, 2005; *Lynch-Stieglitz et al.*, 2007]. From North Atlantic records it is evident that NADW was less dense and was exported at shallower depths during peak glacial conditions in late marine oxygen isotope stage (MIS) 3 and MIS 2 to be replaced by southern sourced waters but that the AMOC was at the same time vigorous [*Böhm et al.*, 2015]. Pronounced glacial perturbations (such as fresh-water inputs from iceberg discharge during Heinrich events), however, were strong enough to diminish or even shut down the AMOC [*McManus et al.*, 2004; *Lippold et al.*, 2012; *Böhm et al.*, 2015], while during interstadials the AMOC remained strong [*Henry et al.*, 2016]. In the SO, in contrast, shallower and reduced

import of warm and saline NADW has been inferred to have led to a higher degree of stratification, which likely acted as a positive feedback mechanism for global cooling during glacial episodes due to enhanced carbon sequestration to the deep ocean [e.g., *Adkins*, 2013; *Yu et al.*, 2016].

Weathering inputs to the oceans from the continents, on the other hand, have also responded to climatic changes on similar time scales. Changes in the hydrological conditions, for instance, influence weathering style and transport mechanisms (aeolian, fluvial, and ice-rafted), while source regions of weathering inputs have changed on both geological and shorter time scales [e.g., *Petschick et al.*, 1996; *Walter et al.*, 2000; *Diekmann et al.*, 2003]. Moreover, there is evidence that increased dust supply may act as a feedback mechanism to climatic changes, serving as fertilizer for marine productivity in the high southern latitudes leading to enhanced CO_2 drawdown [e.g., *Martin*, 1990; *Jaccard et al.*, 2013]. Changes in sources and mechanisms delivering continental inputs to the ocean are thus not only considered to react to changes in climate but also to modify these.

1.1. Background

Combined radiogenic isotope signatures of neodymium (Nd) and hafnium (Hf) have been applied as reliable tracers of water mass mixing, provenance of weathering inputs, and changes in continental weathering regimes [e.g., *Frank*, 2002; *Goldstein and Hemming*, 2003]. In dissolved form, Nd is moderately particle-reactive and has an average oceanic residence time between 360 and 1500 years [*Jeandel et al.*, 1995; *Tachikawa*, 2003; *Siddall et al.*, 2008; *Arsouze et al.*, 2009; *Rempfer et al.*, 2011]. A longer residence time of Hf compared to Nd has been proposed based on relatively homogenous Hf isotope ratios across different ocean basins and its speciation in seawater [e.g., *White et al.*, 1986; *Godfrey et al.*, 2008]. However, more recently evidence emerged that Hafnium is more efficiently adsorbed to particles [*Stichel et al.*, 2012a] and that its residence time in seawater is likely shorter than that of Nd [*Rickli et al.*, 2009; *Firdaus et al.*, 2011; *Stichel et al.*, 2012a; *Chen et al.*, 2013b; *Filippova et al.*, 2017].

Seawater is labeled with the Nd and Hf isotope composition of rocks on the surrounding continents via dissolved weathering inputs by rivers, exchange with particulate material in the water column, or with shelf sediments [e.g., *Lacan and Jeandel*, 2005; *Bayon et al.*, 2006; *van de Flierdt et al.*, 2007; *Rickli et al.*, 2009, 2010] and potentially also via hydrothermal inputs in the case of Hf [*Bau and Koschinsky*, 2006]. Radiogenic Nd and Hf isotopic compositions are given as ε values, which correspond to the normalized differences of the sample ratio from the one of the chondritic uniform reservoir (CHUR) times 10,000 ($^{143}Nd/^{144}Nd_{CHUR} = 0.512638$ [*Jacobsen and Wasserburg*, 1980] and $^{176}Hf/^{177}Hf_{CHUR} = 0.282769$ [*Nowell et al.*, 1998]). The seawater-derived isotopic composition of Nd and Hf extracted from marine sediments has been applied to reconstruct water mass mixing-processes and local weathering inputs to the oceans [e.g., *Piepgras and Wasserburg*, 1982; *Ling et al.*, 1997; *Burton et al.*, 1999; *Piotrowski et al.*, 2000; *Rutberg et al.*, 2000; *Chen et al.*, 2012]. In fact, while Nd isotopes in the intermediate and deep SO essentially reflect water mass mixing, Hf isotopes were demonstrated to be homogenous in the entire Atlantic sector of the SO [*Stichel et al.*, 2012a] and thus are not suitable to trace water mass mixing in this ocean basin.

The modern hydrography of the Atlantic Sector of the Southern Ocean is dominated by northward flowing Antarctic Intermediate Water (AAIW) at intermediate depths (500 to 1000 m, $\varepsilon_{Nd} = -8.5$) and Antarctic Bottom Water (AABW) at abyssal ($\varepsilon_{Nd} = \sim -9$), whereas depths between 2000 and 3500 m are affected by the admixture of less radiogenic northern sourced NADW ($\varepsilon_{Nd} = \sim -11$) [*Stichel et al.*, 2012a] (see Figure 1). The well-mixed Circumpolar Deep Water (CDW) of the Antarctic Circumpolar Current (ACC) also has an ε_{Nd} signature of ~ -9. At the surface, warm and saline water masses entering from the tropical Indian Ocean (Agulhas Current (AC); ε_{Nd} between -7 and -8 [*Stichel et al.*, 2012a]) are separated from cold southern sourced surface waters at the subpolar front (Figure 1). The Agulhas Ridge rising more than 2500 m from the surrounding seafloor is a part of the Agulhas-Falkland Fracture Zone. The ridge basement is of tectono-magmatic origin and was uplifted at least until the early Oligocene [cf. *Uenzelmann-Neben and Gohl*, 2004]. It forms a natural barrier for northward flowing bottom water masses, and its top is located in the mixing zone of modern CDW and NADW.

Seawater Nd isotope records obtained from Fe-Mn crusts and authigenic Fe-Mn oxyhydroxide coatings of bulk sediments and of foraminifera in the deep SO revealed a significantly decreased influence of unradiogenic North Atlantic sourced water masses (Northern Component Water (NCW)) during the last glacial

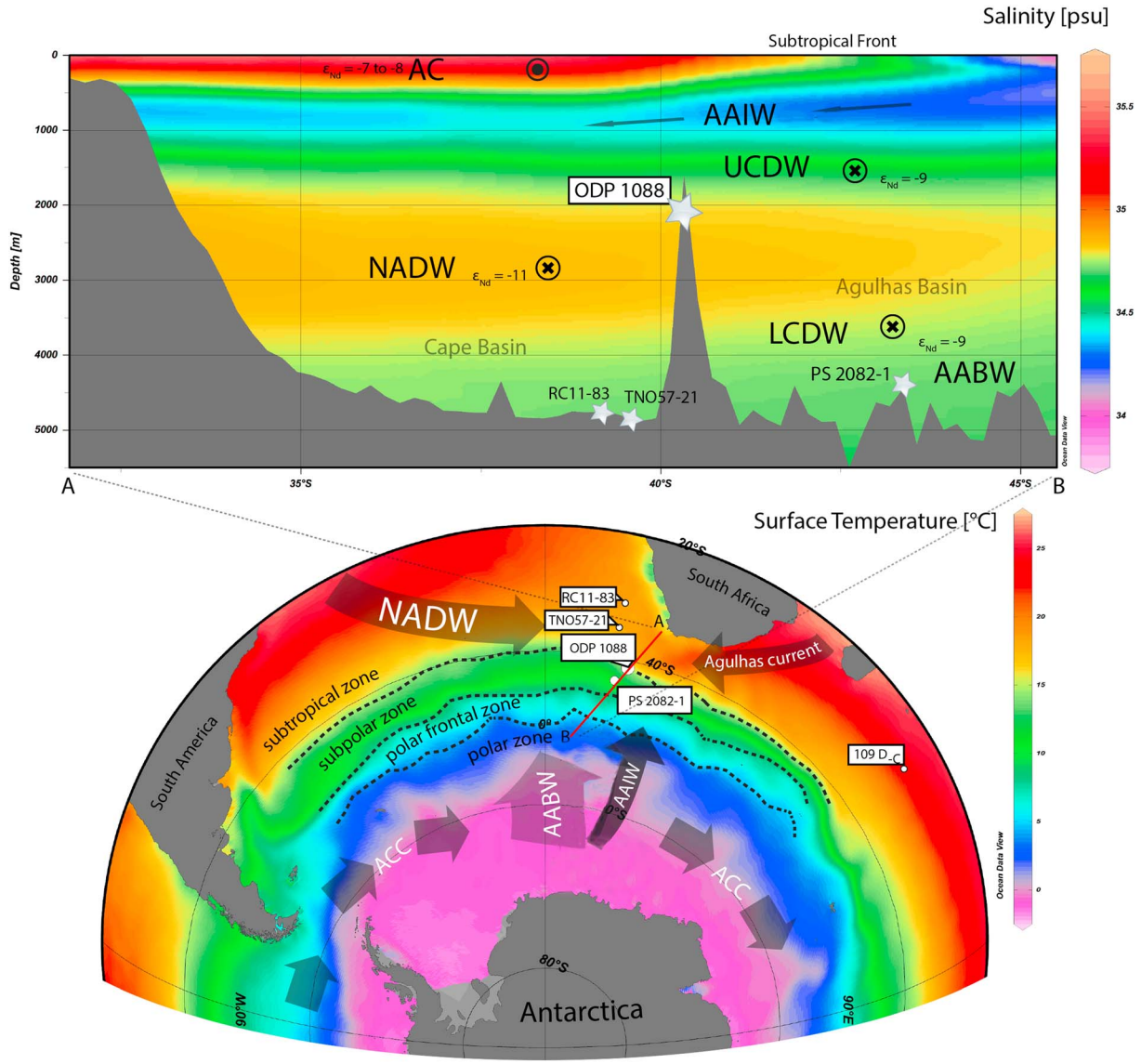

Figure 1. Section and map of the study area showing the locations of ODP Site 1088 and nearby sediment cores and ferromanganese crust samples. Schematic pathways of major water masses of the modern Southern Ocean [*Reid*, 1996] are displayed by grey arrows. The black dashed lines represent approximate locations of oceanic frontal zones [*Orsi et al.*, 1995]. Abbreviations: AABW: Antarctic Bottom Water; AAIW: Antarctic Intermediate Water; AC: Agulhas Current; ACC: Antarctic Circumpolar Current; U/L/CDW: Upper/Lower Circumpolar Deep Water; NADW: North Atlantic Deep Water. Produced using Ocean Data View (Schlitzer, R., Ocean Data View, http://odv.awi.de, 2016).

cycle [*Rutberg et al.*, 2000; *Piotrowski et al.*, 2004, 2008; *Piotrowski*, 2005; *Skinner et al.*, 2013] and during the Mid-Pleistocene Transition (1.2 to 0.7 Ma) [*Pena and Goldstein*, 2014].

Previous studies have also demonstrated that the Lu-Hf and the Sm-Nd isotope-systems behave differently during continental (silicate) weathering and may thus deliver important information on sources and mechanisms of weathering when combined. Distinct relationships for different reservoirs formed during weathering processes such as the "seawater array" [*Albarède et al.*, 1998] and the "clay array" [e.g., *Bayon et al.*, 2009, 2016] emerge when directly comparing radiogenic Nd and Hf isotope signatures. These relationships are based on the fact that very large proportions of a rocks' Hf is bound in zircon minerals, which are very resistant to chemical weathering [e.g., *Balan et al.*, 2001]. Intensified physical weathering (e.g., due to glacial erosion) destroying mineral lattices and increasing mineral surface area available for weathering likely enhances the release of less radiogenic Hf from zircons, causing a higher congruency between bulk rock and dissolved Hf isotope compositions [*Piotrowski et al.*, 2000; *van de Flierdt et al.*, 2002]. Partial dissolution of aeolian and

fluvial transported particles, on the other hand, leads to a particularly incongruent release of Hf isotopes as heavy zircon minerals are lost during transport [e.g., *Rickli et al.*, 2010; *Chen et al.*, 2013b]. Spatial and temporal variations in Hf isotope compositions in seawater have thus been modified by changes in inputs from physical and chemical weathering processes on the close by continents.

Here we present the first data set reconstructing mid-Miocene to Holocene water-mass mixing and continental weathering inputs by using seawater Nd and Hf isotope signatures obtained from sediments on the Agulhas Ridge in the Atlantic sector of the Southern Ocean. This location is ideal to study variations in intermediate depth water mass mixing between the North Atlantic, the Southern Ocean, and the Indian Ocean. These data are further complemented by detrital Nd and Hf isotope signatures reflecting changes in continental weathering inputs. The new data provide the first continuous record of changes in intermediate depth ocean circulation and continental inputs in the Atlantic sector of the Southern Ocean based on radiogenic isotopes since the mid-Miocene, which includes major climatic transitions such as the onset of Northern Hemisphere Glaciation.

2. Material and Methods

2.1. Sedimentology

The studied core of Site 1088 (Ocean Drilling Program (ODP) Leg 177, December 1997), located on the Agulhas Ridge at 41°8.163′S, 13°33.770′E, was recovered from a water depth of ~2082 m reaching a length of 223.4 m. The sediments predominantly consist of carbonate nannofossil foraminiferal ooze with carbonate contents ranging between 80 and 95%, which increase downcore [*Gersonde et al.*, 1999]. While relative abundances of foraminifers are high in the topmost 20 m they decrease progressively downhole and nannofossil percentages increase accordingly. In the section younger than ~2.8 Ma interbeds of darker, less foraminifera-rich sediment (up to 80% foraminifers) commonly incorporate ice-rafted debris (IRD), rare drop stones, and occasionally diatoms. Some of these darker beds also show erosional contacts with the underlying pale nannofossil ooze [cf. *Gersonde et al.*, 1999].

In total, 118 depth intervals were sampled spanning the entire length of the core. However, 80% of all samples were taken in the section younger than 4 Ma, while the remainder of the samples have ages between 14 and 4 Ma.

2.2. Age Model

The initial age model based on calcareous nannofossil biostratigraphy for the entire core was published in the Initial Report of the Shipboard Scientific Party [*Gersonde et al.*, 1999] and was later refined by *Censarek and Gersonde* [2002] and *Marino and Flores* [2002]. The biostratigraphy was extended by tuning benthic foraminiferal (*Cibicidoides*) $\delta^{18}O$ records to the records of *Bassinot et al.* [1994] and *Mix et al.* [1995] for the interval covering the uppermost 1.2 Ma [*Hodell et al.*, 2003a]. In addition, tuning of $\delta^{13}C$ and $\delta^{18}O$ records of planktonic (*Globigerina bulloides*) and benthic (*Cibicidoides*) foraminifers to the records of *Mix et al.* [1995] supports the nanofossil stratigraphy for the interval between 2.5 and 8.6 Ma [*Billups*, 2002; *Billups et al.*, 2008]. Sedimentation rates decrease toward the younger part with an overall range between 30 and 7 m/Myr [*Diekmann et al.*, 2003]. In addition, a hiatus was identified between 12.3 and 12.7 Ma.

2.3. Sample Preparation and Radiogenic Isotope Analysis

2.3.1. Extraction of Bottom Water Signatures From Ferromanganese Oxyhydroxide Coatings of Bulk Sediments

Seawater Nd and Hf isotope signatures (84 samples and 63 samples, respectively) were extracted from authigenic ferromanganese oxyhydroxides of bulk sediment samples (approximately 3 g; freeze-dried) following the leaching protocol of *Gutjahr et al.* [2007]. The carbonate fraction was partly removed by adding 20 mL 2.8 M acetic acid, 1 M Na-acetate (pH ~4) on a shaking table for 2.5 h in order to reduce the amount of the disturbing carbonate matrix (which can result in a less efficient removal of Yb during element separation). The authigenic Fe-Mn oxyhydroxide fraction was subsequently dissolved in 25 mL 0.005 M hydroxylamine hydrochloride, 1.5% acetic acid, and 0.03 M Na-EDTA solution (HH) buffered to pH 4 with suprapure NaOH for 90 min at room temperature (i.e., 10 times diluted relative to concentrations used by *Gutjahr et al.* [2007]). Subsequently, the samples were centrifuged and the supernatants were dried and redissolved for ion exchange chromatography.

2.3.2. Extraction of Bottom Water Signatures From Planktonic Foraminifera

On average, 125 mg of mixed species planktonic foraminifera tests were handpicked from the size fraction >315 μm under a light microscope from 60 freeze-dried and clay-free (wet-sieved) sediment samples. The microfossil shells were subsequently cracked between glass plates to ensure that all chambers were opened and were ultrasonicated several times in deionized water and then in ethanol to ensure the removal of most of the clays and other silicate particles. The carbonates and associated ferromanganese coatings of the samples were then progressively dissolved by stepwise addition of dilute nitric acid. The solution was then centrifuged to ensure removal of smallest detrital particles, and subsequently, the Nd was chemically purified by using the same chromatographic method as above.

2.3.3. Detrital Material

A total of 16 samples were selected for measurement of the detrital Nd-Hf isotope compositions. Bulk sample residues processed to extract seawater signatures (section 2.3.1) were further treated with a stronger reductive leaching solution for 1 day to ensure complete removal of remaining Fe-Mn oxyhydroxides. Afterward, these samples were dried, ground, and 5% H_2O_2 was added for 72 h to oxidize organics that might otherwise disturb chemical purification. The samples were then further treated in aqua regia on a hotplate at 140°C preceding digestion in a mixture of concentrated HNO_3 and HF in steel jacketed high-pressure bombs at ~180–200°C for 4 days.

2.3.4. Chemical Purification and Mass Spectrometry

A cation exchange resin (AG50W-X8) was used to first separate high field strength elements (HFSE) and rare earth elements (REEs). Subsequently, the HFSE and REE cuts were further purified with Ln-spec resin following *Münker et al.* [2001] and *Pin and Zalduegui* [1997], respectively. Hf and Nd isotope compositions were measured at GEOMAR in Kiel on a Nu Instruments multicollector-inductively coupled plasma-mass spectrometer (MC-ICP-MS) (all Nd samples, 20 Hf leachates and all detrital Hf samples) or on a Thermo Scientific Neptune Plus MC-ICP-MS and on a Thermo Scientific Neptune Plus MC-ICP-MS at the ETH in Zurich (43 Hf leachate samples). Instrumental mass bias was corrected applying an exponential mass fractionation law by using a natural $^{179}Hf/^{177}Hf$ ratio of 0.7325 and $^{146}Nd/^{144}Nd$ of 0.7219, respectively. While average Nd yields were ~900 ng in bulk sediment leachates and ~30 ng from foraminifers, Hf yields from sediment leachates were quite low with an average of 13 ng. Blanks were at an average of 0.93 ng for Nd and 0.18 ng for Hf. Respective isotope standards were measured at similar concentrations as samples during each measurement batch. $^{176}Hf/^{177}Hf$ ratios of all samples were normalized to the literature value of JMC475 (0.282160 [*Nowell et al.*, 1998]). while $^{143}Nd/^{144}Nd$ was normalized to the literature value of JNdi-1 (0.512115 [*Tanaka et al.*, 2000]). The 2σ external reproducibilities of the Hf and Nd isotope measurements were in the range of 0.2 to 0.4 ε units (for 50 and 10 ng Hf standards, respectively) and 0.1 to 0.34 ε units (for 50 and 20 ng Nd standards, respectively), respectively.

Since Hf beam intensities were very low for some samples internal uncertainties exceeded the external reproducibility for some of the sediment leachates (see supporting information). The reliability of data produced from these measurements is addressed below. Using a jet sampler and x skimmer cone interface, the sensitivity of the Neptune Plus MC-ICP-MS was sufficient to perform precise and accurate Hf isotope measurements even for solutions containing as little as 1.4 ng Hf. ^{176}Yb interferences on ^{176}Hf were negligible for the samples measured on the Neptune. Nevertheless, Yb-doped standards were used to assure that adequate interference correction was applied. The addition of 1% Yb and 1% Lu (not exceeded in sample solutions) to some of the standards produced an average deviation from the standard value (2σ) 0.14 ε units smaller than the pure Hf standard, hence within measurement uncertainty. An additional correction of Yb interferences was therefore not applied.

3. Results

All ε_{Nd} and ε_{Hf} signatures presented in this study were not corrected for radiogenic ingrowth since deposition. Maximum contribution of decay to both radiogenic isotope systems was calculated to be 0.2 ε units in the oldest samples, which is within analytical uncertainty. Results of all seawater Hf and Nd isotope measurements and their respective uncertainties are presented in Figures 2c and 2f and are summarized in Table S1. Detrital Hf and Nd isotope measurements and their respective uncertainties are presented in Figures 2d and 2g and Table S1.

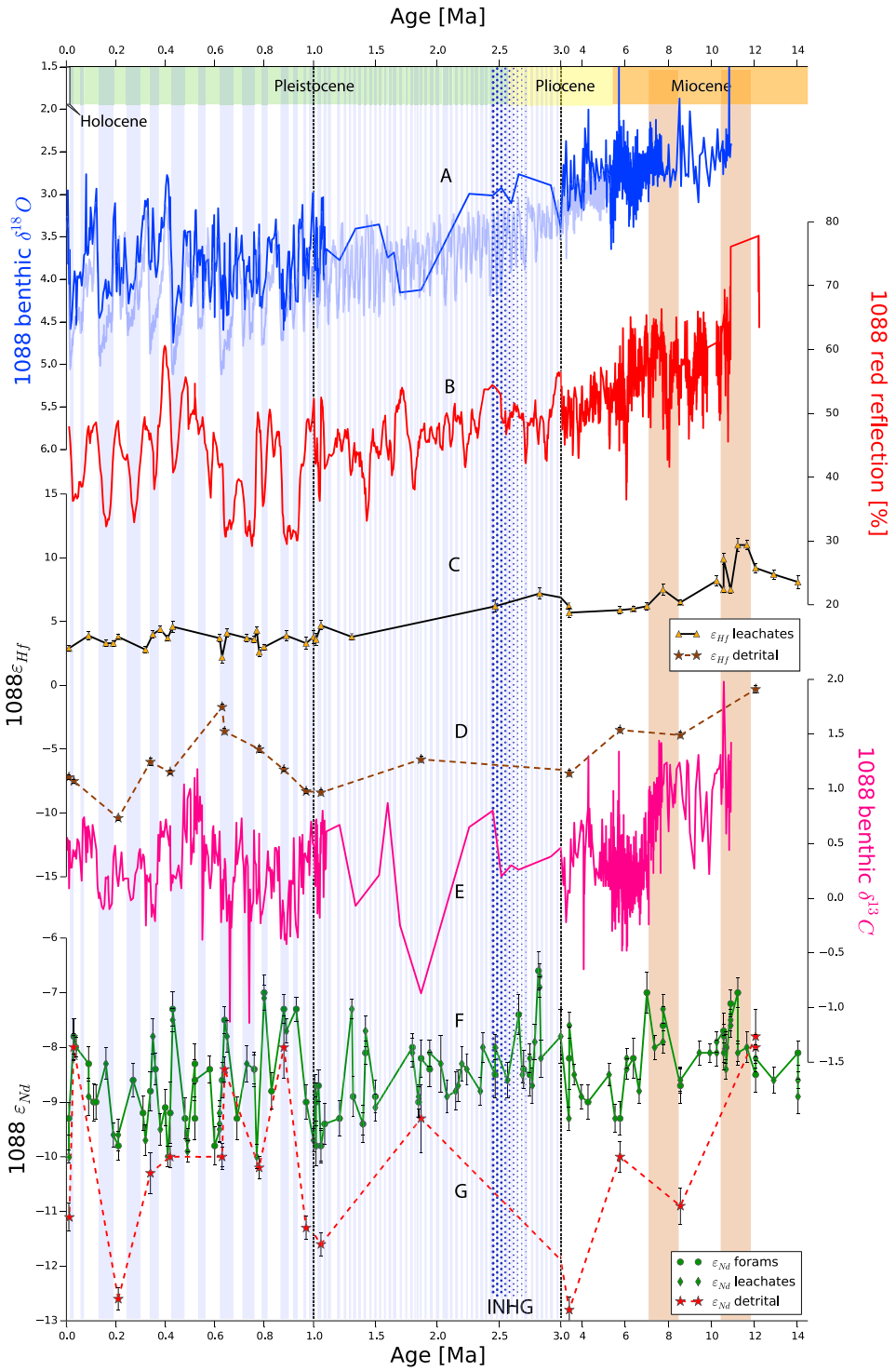

Figure 2. Temporal evolution of geochemical proxies in ODP Site 1088 from the Agulhas Ridge. (a) Benthic oxygen isotope time series obtained from *Cibicidoides* [*Billups*, 2002; *Hodell et al.*, 2003a; *Billups et al.*, 2008]. In the background the global benthic oxygen isotope evolution is plotted and the global marine isotope stages are displayed as blue bars [*Lisiecki and Raymo*, 2005]. (b) Sediment color expressed as reflectance of red visible light with wavelength of 650–750 nm [*Gersonde et al.*, 1999]. (c) Seawater Hf isotope time series from ODP 1088 (this study). (d) Detrital Hf isotope time series from ODP 1088 (this study). (e) Benthic carbon isotope time series *Cibicidoides* [*Billups*, 2002; *Hodell et al.*, 2003a; *Billups et al.*, 2008]. (f) Seawater Nd isotope time series from ODP 1088 (this study). (g) Detrital Nd isotope time series from ODP Site 1088 (this study). The error bars denote the 2σ external reproducibility of the ε_{Hf} and ε_{Nd} measurements. Note that the age scale on the *x* axis changes at 3 and 1 Ma.

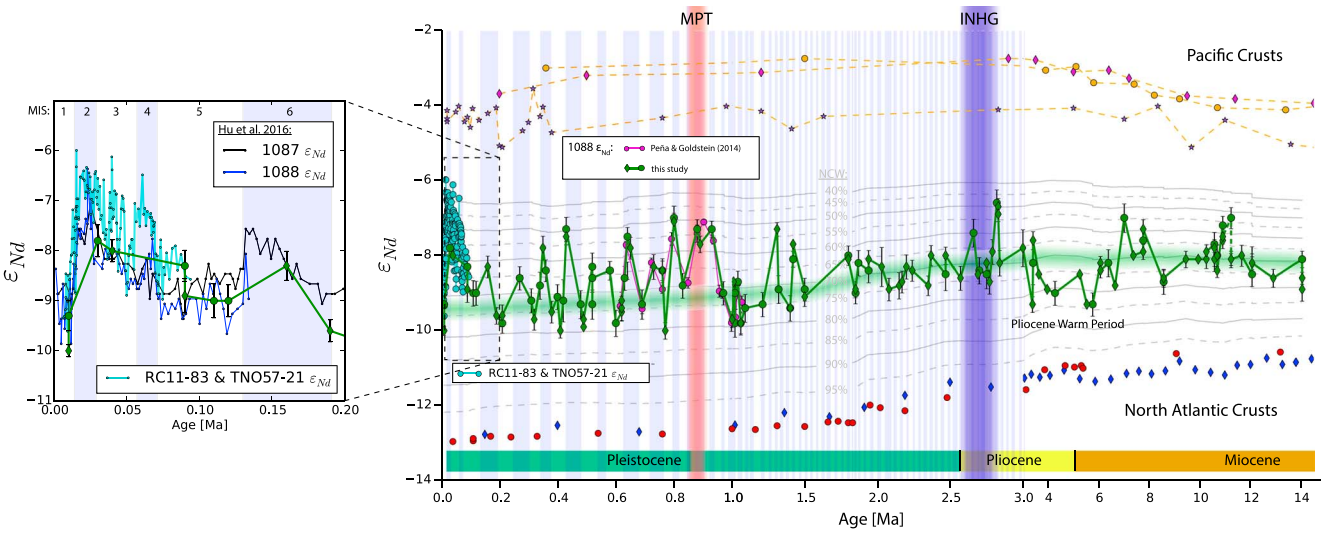

Figure 3. Comparison between the seawater Nd isotope evolution of the intermediate depth Southern Ocean at ODP Site 1088 [*Pena and Goldstein*, 2014; *Hu et al.*, 2016; this study] and compositions of the North Atlantic [*O'Nions et al.*, 1998; *Burton et al.*, 1999] and Pacific Ocean [*Abouchami et al.*, 1997; *Ling et al.*, 1997] end-members, as well as near-by late Quaternary records of cores RC11-83 and TNO57-21 from the deep Cape Basin [*Piotrowski et al.*, 2008]. The grey lines represent calculated mixing proportions of North Atlantic sourced water (NCW) with Pacific sourced water (SCW) according to the variable end-member Nd compositions and constant Nd concentrations of $[Nd]_{NCW} = 22$ pmol/kg and $[Nd]_{SCW} = 42$ pmol/kg [*Goldstein and Hemming*, 2003]. The error bars denote the 2σ external reproducibility of the ε_{Nd} measurements. Note that the age scale changes at 3 and 1 Ma.

3.1. Seawater Nd Isotope Signatures

The ε_{Nd} values of all samples ranged between −10 and −6.6 at an average external reproducibility of 0.29 (2σ) (Figures 2 and 3). The ε_{Nd} values of samples older than ~1 Ma varied within a narrower range of −8 ± 1.5. Thereafter, values dropped to less radiogenic values averaging −9 ± 1. The Holocene ε_{Nd} values of our record (−10) matched modern seawater from a nearby location (−9.9; Station 101 of *Stichel et al.* [2012a]). In general, our ε_{Nd} time series oscillated in harmony with marine isotope stages (MIS) [*Lisiecki and Raymo*, 2005] in that more radiogenic values prevailed during glacial stages than during interglacial stages. For samples older than 1 Ma it was more difficult to unambiguously assign particular MIS. The covariation of ε_{Nd} with color reflectance, however, was still very clear and served to identify glacial and interglacial period. A pronounced maximum ($\varepsilon_{Nd} = -6.6$) consisting of two data points occurred at about 2.8 Ma. Furthermore, we observed two pronounced positive ε_{Nd} peaks during the middle to late Miocene (around 11 Ma and between 7.7 and 7 Ma, marked with brown dashed fields in Figure 2).

The Nd isotope data of bulk sediment leachates and foraminifera were identical within the 2σ uncertainties. Only one sample from the mid-Miocene corresponding to an age of 11.2 Ma showed a larger offset of 1.1 ε_{Nd} units, with the foraminiferal ε_{Nd} being more radiogenic than that of the bulk sediment leachate, which is likely caused by inhomogeneity of the sediment material of this one sample. The data obtained from the leachate and foraminifera thus both reliably reflect past bottom water signatures.

3.2. Detrital Nd Isotope Signatures

All detrital ε_{Nd} values ranged between −13 and −8, with only 5 of the 16 samples being more radiogenic than −10, and thus were generally less radiogenic than the respective seawater fractions. However, in particular, during the Pleistocene, the detrital ε_{Nd} signatures varied with the climatic stages similar to the seawater Nd isotopes, in that more radiogenic signatures reflected glacial stages (Figure 2).

3.3. Seawater Hf Isotope Signatures

The seawater ε_{Hf} signatures ranged from highly radiogenic +12.5 to unradiogenic +1.9. There was a clear secular trend from more radiogenic compositions (+5.5 to +12.5) in the Miocene and early Pleistocene (3 to 13 Ma) to a relatively uniform Hf isotope composition between +2 and +5 over the last 3 Myr. While the ε_{Hf} signatures exhibited three radiogenic peaks at ~11.2 Ma, 7.3 Ma, and 2.8 Ma interrupted the

otherwise steady decline in the Miocene and Pliocene, they reached values 1.5 Myr ago. The average ε_{Hf} composition of this stable episode (+3.5 ± 0.9) agreed with that of the nearest measured modern seawater sample (+3.5 ± 0.8, 2000 m water depth, St. 104 [*Stichel et al.*, 2012a]).

3.4. Detrital Hf Isotope Signatures

The contrasts between detrital and authigenic ε_{Hf} values were more pronounced than those of ε_{Nd}. Although the detrital Hf isotope signature was generally much less radiogenic than seawater with values ranging from −10.4 to −0.3, its evolution has been parallel to seawater with the exception of an excursion to more radiogenic detrital values between 1 and 0.4 Ma.

4. Discussion

4.1. The Role of Nonconservative Nd Behavior

Before we interpret our data in terms of bottom seawater variability controlled by deepwater mass mixing we have to consider that nonconservative effects may have biased the isotopic compositions of bottom waters. Boundary exchange in shelf and/or continental rise settings [*Lacan and Jeandel*, 2005; *Arsouze et al.*, 2009; *Rempfer et al.*, 2012] or the presence of easily dissolvable volcanic ashes and/or high amounts of IRD in the sediment [e.g., *Wilson et al.*, 2013; *Roberts and Piotrowski*, 2015; *Blaser et al.*, 2016] can potentially alter seawater isotopic compositions and, hence, authigenic sedimentary signatures. While the key controls driving the effects and strength of boundary exchange at a given location are still not well understood, it is likely that the resulting effects were stronger during phases of sluggish AMOC [e.g., *Lang et al.*, 2016] and may thus have modified seawater ε_{Nd} to variable degrees across G-I cycles. Considering that detrital and authigenic Nd signatures varied in parallel during some periods of time of our record we cannot fully exclude slight shifts of the extracted seawater signatures originating from exchange with the detrital fraction of the sediments or even contributions from the pore waters [*Abbott et al.*, 2015]. We stress, however, that modern ambient deepwater ε_{Nd} were successfully captured supporting our bulk sediment leaching approach. In addition, the Nd isotope signatures of the bulk sediment leachates and corresponding foraminifera agree for most of the data. This is consistent with the location of our core site at a large distance to continental landmasses and reactive sediment input from land.

Volcanic ash was mainly observed in the interval between 6.3 and 7.3 Ma but is present in small amounts in many sections of this core [*Gersonde et al.*, 1999]. Even though it is unlikely that the seawater Nd isotope composition was altered by instantaneous release of Nd from volcanic ash over an extended period of time, it is possible that volcanic-ash-derived Nd was released during the bulk sediment leaching [*Wilson et al.*, 2013; *Blaser et al.*, 2016]. However, we expect such contamination by volcanic material to be negligible as indicated by our measurements performed on foraminifera tests which are clearly not influenced by volcanic ash particles.

4.2. Variations in AMOC Strength During the Last 14 Ma Inferred From Nd Isotope Evolution

At present, the Nd isotope signature of the waters above the Agulhas Ridge reflects essentially conservative mixing between NCW (NADW) and CDW, the Nd composition of which is ultimately controlled by admixture of both Pacific and Atlantic sourced waters with negligible contributions from boundary exchange with the Antarctic continent [*Carter et al.*, 2012; *Stichel et al.*, 2012a]. We therefore assume binary mixing between water masses delivered from the North Atlantic (NCW) with water mass delivered from the Pacific (Southern Component Water (SCW)) to have prevailed over the past 14 Myr.

Following the binary mixing model of *Piotrowski et al.* [2004] modern SO seawater ε_{Nd} is the product of a NCW-SCW mixture of about 3:1. These calculations are based on ε_{Nd} signatures of modern NCW of −13.5 and −4.5 for SCW together with Nd concentrations $[Nd]_{NCW} = 22$ pmol and $[Nd]_{SCW} = 42$ pmol [*Goldstein and Hemming*, 2003]. In the present study it is assumed that water masses with these compositions have been mixed conservatively in the SO and inputs from exchange processes with the ocean boundary on their respective pathways did not significantly affect NCW and SCW Nd isotope ratios and concentrations [cf. *Piotrowski et al.*, 2004, and references therein]. Holocene samples in our record ($\varepsilon_{Nd} = -10$ to −9.3) agree very well with the modern seawater composition of the SO of ~ −9.9 measured at a depth of 2000 m in the Cape Basin close to the Agulhas Ridge [*Stichel et al.*, 2012a], indicating that the location experienced no resolvable addition from preformed ferromanganese phases of continental origin. This is in contrast, for

instance, to the Angola Basin where Congo-derived ferromanganese phases have been shown to contribute significantly to the authigenic fraction of the sediments [*Bayon et al.*, 2009].

In order to reconstruct changes in the Nd isotope compositions of Pacific and Atlantic sourced waters through time, Fe-Mn crust data from the North Atlantic [*O'Nions et al.*, 1998; *Burton et al.*, 1999] and Pacific [*Abouchami et al.*, 1997; *Ling et al.*, 1997] were used to assess the evolution of the end-member Nd isotopic compositions at a coarse (>100 kyr) temporal resolution (Figure 3). Past variations in end-member Nd concentrations, however, cannot be constrained given that there is currently no proxy for past seawater Nd concentrations. Systematic changes in the concentrations over time cannot be ruled out and have to be considered as a source of uncertainty. In order to quantify these uncertainties, we have tested the impact of changes $[Nd]_{SCW}/[Nd]_{NCW}$ on our calculations by simulating deviations from the current concentration ratio by up to 20%. These simulations show that an increase in $[Nd]_{SCW}$ by 20% translates into a 4% increase of NCW advection, while an increase of the Nd concentration in NCW by 20% translates into a 5% decrease in NCW advection.

Our reconstructions show that the mid-Miocene to Holocene proportions of NCW oscillated between a minimum of 49% and a maximum of 84%. The average of the entire time series of 69% NCW is close to the Holocene composition ranging between 72 and 78%$_{NCW}$, suggesting that general oceanographic configuration has remained similar to today. This 69% NCW contribution is thus considered the baseline of similar-to-modern SO water mass mixing at the Agulhas ridge. These records hence corroborate earlier suggestions [e.g., *Scher and Martin*, 2008] that water masses from the North Atlantic have been advected to the SO in significant amounts since at least the mid-Miocene. Clearly, however, there were pronounced glacial/interglacial differences in AMOC strength over the past 3 Myr and distinct episodes with significantly different mixing proportions stand out in our record and will be discussed in chronological order in the following sections.

4.2.1. Miocene to Pliocene AMOC Variability

During the mid-Miocene (14 to 6 Ma; orange background in Figure 2) the intermediate depth SO Nd isotope composition only showed a relatively small variability of ±0.6 ε_{Nd} units (1 SD) around a mean value of −8.1. The Oligocene and early Miocene long-term trend of decreasing ε_{Nd} described by *Scher and Martin* [2008] did not continue until the older parts of our record. Consistent with interpretations of *Scher and Martin* [2004], who measured an $\varepsilon_{Nd}(t)$ of ~ −8.5 for the early Miocene in fossil fish teeth from ODP Site 689 from the Maud Rise, the resemblance of our Miocene data to modern SO mixing proportions suggests an Atlantic circulation pattern similar to modern conditions. Maximum NCW contributions (minimum ε_{Nd} values in Figure 3) in the middle to late Miocene were of the same order as during the Pleistocene interglacials and the Holocene. Analogous to observations of *Scher and Martin* [2008], we did not find any correlation of our data with potentially changing weathering inputs during major drops in eustatic sea level, which are attributed to Antarctic glaciation events [cf. *Miller et al.*, 1998].

Moreover, radiogenic ε_{Nd} peaks at 11.2 Ma and between 7.7 and 7 Ma, which translate into intervals of low NCW admixture of about 60%, are in the same range as ε_{Nd} peaks throughout the entire section and are thus considered robust evidence for reduced NCW import during these episodes. Low NCW admixture between 8 and 7 Ma is consistent with conclusions drawn from $\delta^{13}C$ gradients between the SO, the North Atlantic, and the Pacific [*Billups*, 2002].

Similar to the observations of *Billups* [2002], our record suggests a stronger late Miocene AMOC preceding a global warm period at 6 Ma that was possibly amplified by the shoaling of the Central American Seaway [*Haug and Tiedemann*, 1998] and/or by the widening of the Arctic-Atlantic gateway [*Knies et al.*, 2014].

Between 6 and 3 Ma enhanced NCW export to the Southern Ocean resulted in an average of 76%$_{NCW}$ and was thus up to 10% stronger than the modern interglacial circulation mode. More radiogenic ε_{Nd} values above −8, indicating weaker NCW export, were only reached again close to the end of this period. These observations are in good agreement with interpretations of *Billups* [2002] who, based on a compilation of benthic $\delta^{13}C$ records from the North Atlantic, Pacific, and SO, inferred enhanced admixture of a northern sourced water mass similar to modern NCW near 6.0 Ma and in excess of the modern admixed proportions during the early Pliocene at ODP Site 1088. With global mean temperatures of up to 3.5°C warmer and atmospheric CO_2 levels about 35% higher than the preindustrial value the early and mid-Pliocene have been identified as a time of prolonged warmth associated with a vigorous AMOC [e.g., *Raymo et al.*, 1996; *Martínez-Botí et al.*, 2015].

In contrast to the benthic $\delta^{13}C$ record of the same core, our Nd isotope time series suggests a return to reduced AMOC strength in the late Pliocene (around 3 Ma) as indicated by a trend to more radiogenic ε_{Nd} marking the transition into an episode of global cooling.

4.2.2. The Intensification of Northern Hemispheric Glaciation

At 2.8 Ma maximum ε_{Nd} values of −6.6 (Figure 4b) mark a pronounced weakening of the AMOC with NCW percentages below 50%. Consequently, the relative fraction of SCW in the SO increased by about a factor of 2 compared to its average proportion (from $25\%_{SCW}$ to more than $50\%_{SCW}$). At this time, the Northern Hemisphere experienced a major acceleration in the buildup of continental ice shields (see Figure 4e) known as the Intensification of Northern Hemispheric Glaciation (~3.6–2.4 Ma [*Raymo*, 1994]). An age control point at 2.84 Ma for 27.54 meters composite depth (mcd) [*Billups et al.*, 2008] decreases the age uncertainty (control point spacing 300–400 kyr [*Billups et al.*, 2008]) to only a few thousand years for the ε_{Nd} peak at 2.82–2.83 Ma (27.3–27.4 mcd). Furthermore, color reflection data from the same core (Figure 4a) clearly document glacial or interglacial stages (low reflections and low carbonate content typically mark glacial stage conditions and vice versa). Consequently, we are confident to assign the observed ε_{Nd} peak to glacial MIS G10, which has previously been identified as the first glacial marked by buildup of large ice sheets in the Northern Hemisphere [*Jansen et al.*, 2000].

Comparison of evidence for marked incursions of SCW to the North Atlantic based on Nd isotope data obtained from core U1313 (situated in the core of modern NADW at 41°N, 32.5°W and a depth of 3426 m) shows that the shift of 1.6 ε_{Nd} units (from −13.1 to −11.5 [*Lang et al.*, 2016]) (Figure 4c) triggered by the incursion of SCW into the North Atlantic during MIS G10 was identical to that observed in our ε_{Nd} record (from −8.2 to −6.6; Figure 4b). This supports rapid SCW expansion delivering more radiogenic Nd signatures to the North Atlantic accompanied by a reduction of NCW. *Lang et al.* [2016] have argued for a connection of changes in deepwater circulation and global climate to be driven by the interplay of Southern Ocean conditions, notably deepwater densification through increased sea ice formation [*Ferrari et al.*, 2014] versus northern forcing agents such as a reduction in NCW formation during the glacials due to its sensitivity to freshwater forcing in the North Atlantic [*Böhm et al.*, 2015].

4.2.3. The Transition to the Modern Icehouse World

Between 2.8 and 1.5 Ma, the variability of the ε_{Nd} signatures was limited around a mean value of -8.4 ± 0.4, corresponding to a NCW percentage of $71 \pm 6\%$. The invariance observed in our ε_{Nd} record suggests a time of a stable and strong AMOC in this section on glacial interglacial time scales. This further indicates that glacial conditions during this episode did not significantly reduce the export of northern sourced water masses, consistent with a strong but shallow deepwater formation cell suggested by benthic carbon isotope data in the North Atlantic covering the latest Pliocene/early Pleistocene [*Venz and Hodell*, 2002].

After 1.55 Ma a marked decline of glacial $\delta^{13}C$ values was recorded in the Southern Ocean [*Hodell and Venz*, 1992; *Venz and Hodell*, 2002] as well as in the deep North Atlantic [*Raymo et al.*, 1990]. These shifts were attributed to a major reorganization in deep circulation patterns of the North Atlantic, also documented by ε_{Nd} records from the northeast Atlantic [*Khélifi and Frank*, 2014]. Based on a significant shift of interglacial bottom water ε_{Nd}, *Khélifi and Frank* [2014] suggested a diminished production of well-ventilated deep waters in the Nordic Seas between 1.6 and 1.4 Ma. This in turn may have lead to a major reduction in NCW production and export to the SO. Revealing first major cyclic radiogenic excursions directly after 1.5 Ma, our ε_{Nd} record adds new evidence for diminished glacial NCW admixture (resulting in SO proportions as low as $50\%_{NCW}$) after 1.5 Ma, marking the transition to late Quaternary glacial-interglacial variability.

Between 1.2 and 0.9 Ma, our Nd isotope record confirms a phase of strong AMOC during both glacials and interglacials consistent with previous observations by *Pena and Goldstein* [2014]. The Nd isotope data translate into high NCW proportions of 70–80% in the intermediate-depth SO at the time (Figures 2f and 3). This is consistent with $\delta^{13}C$ records from the North Atlantic, indicating that the glacial-interglacial variability in AMOC strength was very low from ~1.1 to 0.9 Ma [*Venz and Hodell*, 2002].

From the "Thermohaline Circulation Crisis" described by *Pena and Goldstein* [2014] to the present, the AMOC system operated in the modern G-I oscillation mode including strong reductions in NCW export to the SO by up to 40% during glacials [cf. *Rutberg et al.*, 2000; *Piotrowski et al.*, 2004; *Piotrowski*, 2005; *Pena and Goldstein*, 2014].

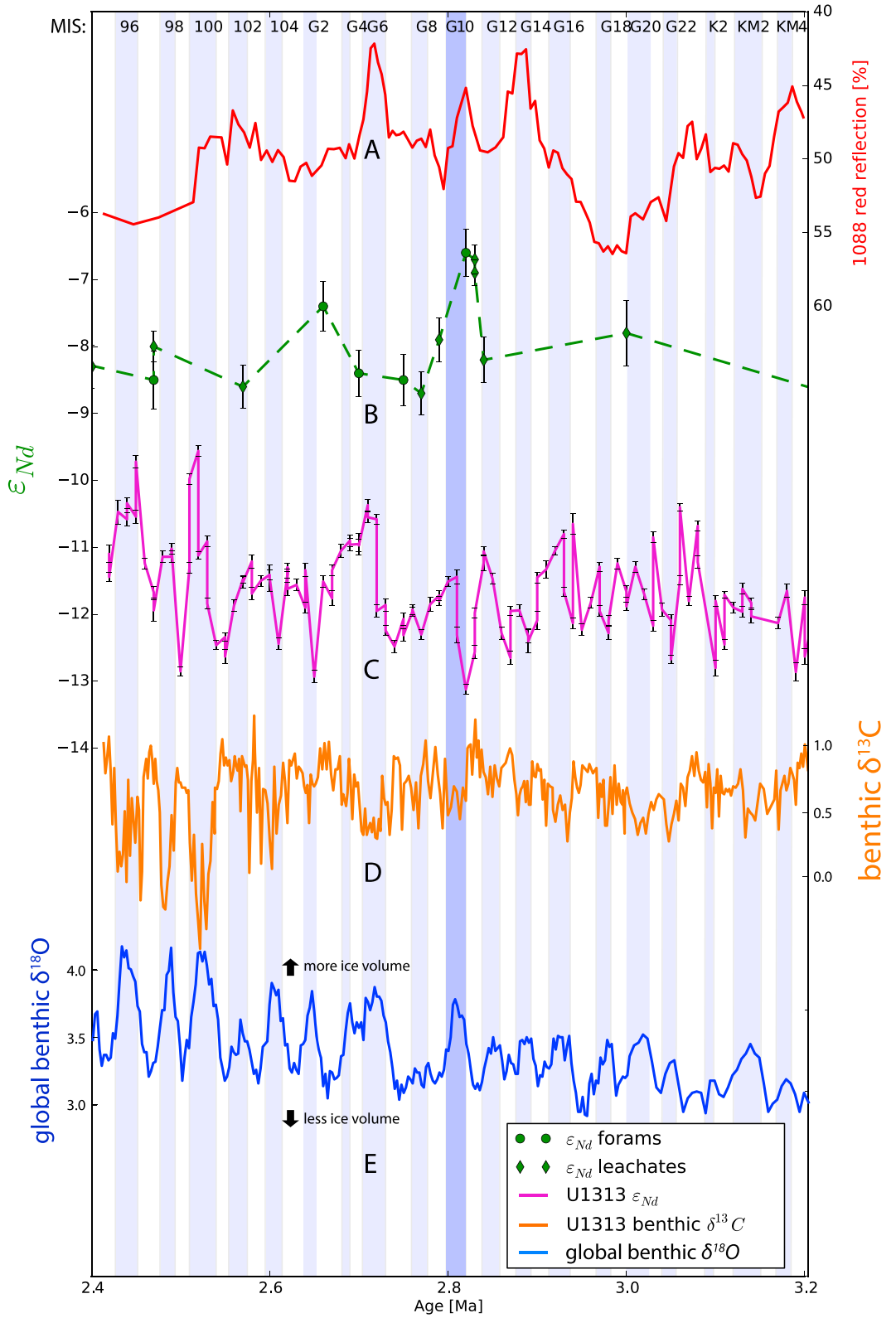

Figure 4. (a) Late Pliocene to early Pleistocene (3.4–2.2 Ma) comparison of sediment color. Nd isotope data from (b) Southern Ocean ODP Site 1088 (this study) and (c) North Atlantic IODP Site U1313 [*Lang et al.*, 2016], (d) the benthic carbon isotope record of U1313 [*Lang et al.*, 2014] and (e) the global benthic oxygen isotope stack [*Lisiecki and Raymo*, 2005]. The error bars denote the 2σ external reproducibility of the ε_{Nd} measurements.

In coherence with a recent study by *Hu et al.* [2016] that includes higher-resolution Nd isotope data of the same core, our new MIS 2 ε_{Nd} value of intermediate waters from the Agulhas Ridge was less radiogenic by up to ~2 ε_{Nd} units than records from the deep Cape Basin (RC11-83 and TNO57-21; see insertion in Figure 3), indicating a higher glacial contribution of NCW to the intermediate waters at the Agulhas Ridge relative to the deep waters in the surrounding deep basins. The Holocene and MIS 3 interglacial ε_{Nd} values, on the other hand, were identical in the deep Cape Basin and the intermediate waters at the Agulhas Ridge. These observations reflect the (modern) interglacial state of vigorous mixing of essentially the entire water column of the SO. Moreover, this confirms previous findings pointing toward reduced glacial NCW advection to shallower depths and a more persistent influence of NCW in the upper circulation cell (above ~3500 m) in the Southeast Atlantic [*Hodell et al.*, 2003b; *Adkins*, 2013; *Hu et al.*, 2016].

4.3. Changes in Regional Oceanography and Weathering Conditions on the Surrounding Continents

4.3.1. Invigoration of Regional Circulation and Long-Term Change in Sediment Provenance

Terrestrial material supplied to the Southern Ocean from Antarctica, Southern Africa, and South America is redistributed by ocean currents at all depths [*Hegner et al.*, 2007]. Understanding sources and pathways thus helps to reconstruct regional ocean current patterns and inputs, which have been related to enhancements of micronutrient release and thus of the fuelling of the biological pump [e.g., *Martin*, 1990; *Jaccard et al.*, 2013].

Radiogenic isotopes of Nd, Sr, and Pb together with other proxies such as clay mineral composition [e.g., *Petschick et al.*, 1996; *Diekmann et al.*, 2003] are commonly used to determine detrital provenance and have been applied to identify shifts in sediment provenance in the Atlantic sector of the SO over the last glacial cycle [e.g., *Walter et al.*, 2000; *Noble et al.*, 2012]. In general, the less radiogenic Nd isotope end-member represents inputs from South Africa and eastern Antarctica, while the more radiogenic end-member mainly originates from Patagonia/South America and western Antarctica. More radiogenic detrital ε_{Nd} during glacial stages have been interpreted as increased glaciogenic continental inputs from Patagonia and West Antarctica imported via the strong ACC or via dust deposition, whereas during interglacial stages sediment inputs from Southern Africa supplied mainly via the Agulhas Current were clearly dominant [*Franzese et al.*, 2006]. The ODP Site 1088 detrital ε_{Nd} signal younger than 1 Ma shows a G-I cyclicity analogous to the observations for the last glacial cycle [*Noble et al.*, 2012] with more radiogenic values during phases of relatively weak AMOC (see Figure 2g) lending further support to the above-mentioned climate-dependant variations in regional-scale circulation dynamics. Changes in detrital Nd isotope signatures recorded by the Pliocene and Miocene sediments, on the other hand, do not correlate well with AMOC variability, suggesting that a different mode of detrital sediment transport prevailed at that time.

In addition to that, detrital Hf isotope signatures (Figure 5f), can also be applied as a sensitive proxy for changes in grain size and thus transport pathways. A trend toward more radiogenic Hf is commonly expected with decreasing grain size in marine sediments, mainly caused by zircon loss during (long distance) sediment transport [e.g., *Vervoort et al.*, 1999, 2011; *Bayon et al.*, 2009, 2016; *Chen et al.*, 2013a]. In agreement with increasing amounts of silt in 1088 sediments over time [*Diekmann et al.*, 2003] (Figure 5b) we observe a continuously decreasing trend in our detrital ε_{Hf} record across the Miocene and Pliocene, which is reflected by a change from the clay array toward the terrestrial array in ε_{Hf}-ε_{Nd} space (green arrow in Figure 6) [cf. *Bayon et al.*, 2016]. For the age interval between 1 and 0.6 Ma the general trend in Figure 5e is reversed before it declines again until the Holocene, which is also reflected in the grain-size record although not as pronounced.

Accordingly, it is highly likely that variations in the admixture of sediment sources represent the first-order control on detrital ε_{Hf}. Analogous to Nd isotopes, the radiogenic compositions in the older parts of the record (detrital $\varepsilon_{Hf} = -1$ to -3) are in theoretic agreement with a distant South American/Patagonian provenance (also more radiogenic due to the presence of relatively young volcanic rocks from the Andean Belt), while the less radiogenic compositions in the younger sections (detrital $\varepsilon_{Hf} = -12$ to -10) represent a proximal South African provenance (predominantly old cratonic rocks with unradiogenic Hf signatures).

Consequently, we infer that the evolution of detrital Hf isotopes represents a combination of the effect of coarsening sediments (Figure 5b) induced by the invigoration of regional ocean circulation (namely, the Agulhas current [*Diekmann et al.*, 2003]) and hence a simultaneous transition in sediment provenance

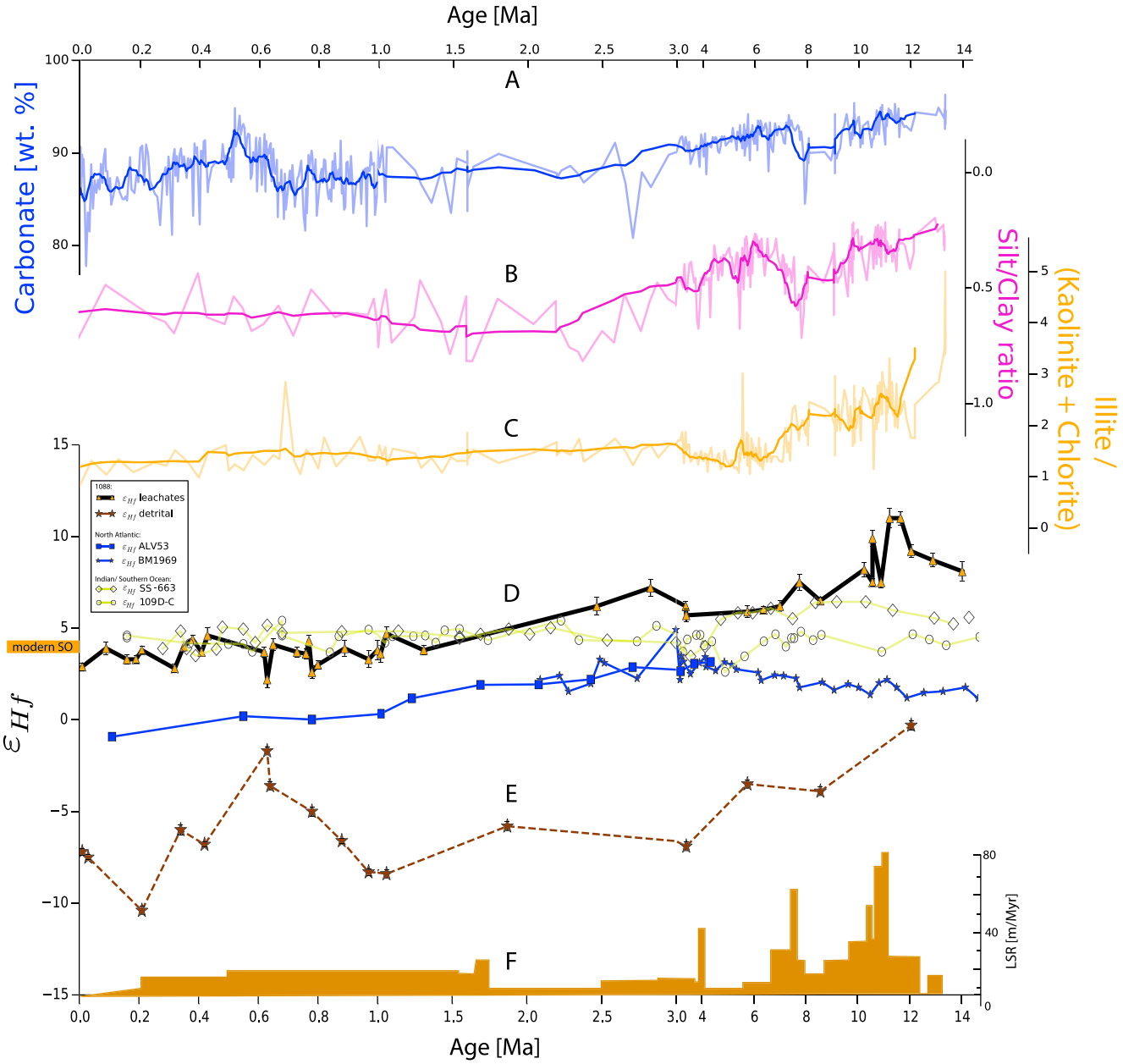

Figure 5. Variability of (a–c) ODP Site 1088 sedimentary components [*Diekmann et al.*, 2003] and the (d and e) Hf isotope record. Authigenic Hf isotope records from crusts from the North Atlantic, equatorial Indian Ocean, and the Indian sector of the Southern Ocean [*Piotrowski et al.*, 2000, 2009] are also shown in Figure 5d. (f) The linearly interpolated sedimentation rate record (LSR) of ODP Site 1088 [*Diekmann et al.*, 2003] is shown. The error bars denote the 2σ external reproducibility of the ε_{Hf} and ε_{Nd} measurements. Note that the age scale changes at 3 and 1 Ma.

from South America/Patagonia to the African craton, which was also inferred from clay mineral assemblages of the same core (Figure 5c) [*Diekmann et al.*, 2003].

4.3.2. Sources and Implications of Seawater Hf Isotope Changes

Previous studies have focussed on marine Hf isotopes as indicators of changes in climatic conditions and thus weathering regimes on nearby continents [*van de Flierdt et al.*, 2002; *Gutjahr et al.*, 2014; *Dausmann et al.*, 2015; *Bayon et al.*, 2016]. Consequently, the presence of ice sheets on the surrounding continents is expected to lead to decreases of the marine ε_{Hf} signatures, which has been observed in Fe-Mn crust records from the Arctic Ocean [*Dausmann et al.*, 2015], as well as in Fe-Mn crust records [*Piotrowski et al.*, 2000] and Late Quaternary sedimentary records from the North Atlantic [*Gutjahr et al.*, 2014]. Moreover, recent work by *Bayon et al.* [2016] demonstrated the relationship between climatic conditions (temperature and

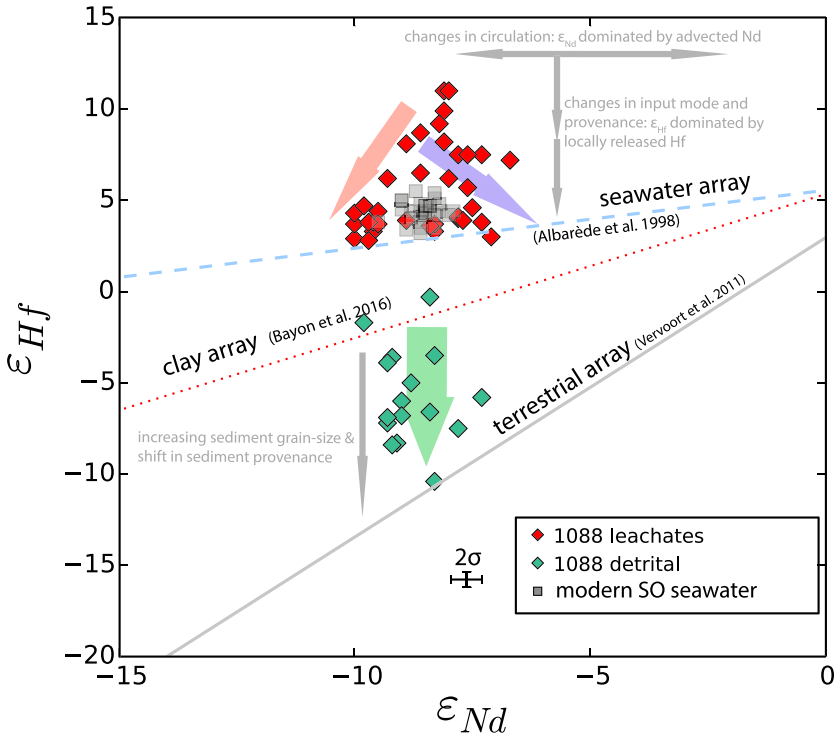

Figure 6. Cross-plot of seawater and detrital Hf and Nd isotope compositions from the Southern Ocean of the past 14 Myr. The dashed line represents the global seawater array defined by Fe-Mn crust and seawater data [*Albarède et al.*, 1998]. The solid grey line represents the global terrestrial array [*Vervoort et al.*, 1999]. The red dotted line represents the clay array [*Bayon et al.*, 2016]. The red arrow represents the temporal evolution of weathering inputs from the surrounding continents during interglacial conditions from highly incongruent in the Miocene to more congruent in the Pleistocene. The blue arrow expresses the development during glacials reflecting the changes in NCW advection affecting the seawater Nd isotope compositions. The green arrow represents the evolution of the detrital material related to both changes in grain-size distributions and provenance of the sediment. Error bars denote the 2σ external reproducibility of the ε_{Hf} and ε_{Nd} measurements.

precipitation) and congruency in Hf weathering. Accordingly, a large-scale global cooling potentially favors the release of more unradiogenic Hf.

In the modern SO, however, there is no evidence for the predominant release of unradiogenic Hf from the close-by glaciated regions of Eastern Antarctica [*Stichel et al.*, 2012b] and Western Antarctica [*Rickli et al.*, 2014]. In addition, there is no indication for the presence of large ice sheets and glaciers on the nearby Southern African continent over the past 14 Myr. Considering the relatively short residence time of Hf in the SO, as inferred from recent seawater studies in the Atlantic Ocean pointing to high rates of scavenging and the lack of enrichment in deepwater Hf concentrations [*Rickli et al.*, 2009, 2010, 2014], the admixture of distal sourced Hf (e.g., from South American runoff) is unlikely.

In agreement with this evidence, our seawater Hf isotope record from the Agulhas Ridge does not exhibit systematic G-I variations during the Pleistocene, clearly showing that seawater Hf isotope signatures have not been sensitive to glacial to interglacial variations of circulation or weathering inputs in the Atlantic sector of the SO over the past 14 Myr. Furthermore, there is no evidence for climatic variations (temperature and precipitation) related to global cooling during glacials on the close-by continents.

Instead, the Hf isotopic compositions (Figure 5d) continuously decreased from highly radiogenic values of up to +11 and an average of +8 during the Miocene and early Pliocene to reach stable conditions in the Pleistocene near the modern day ε_{Hf} of seawater above the Agulhas Ridge (+3.5; 2000 m St. 104 [*Stichel et al.*, 2012a]).

Based on these observations, we infer that the SO seawater evolution toward less radiogenic dissolved Hf isotopic ratios was not caused by the evolution of a more congruent mode of weathering. The highly

radiogenic Hf isotope compositions in the early part of the record, which apparently indicate strongly incongruent weathering conditions (Figure 6), were most likely caused by aeolian supply and partial dissolution of young volcanogenic particles supplied from Patagonia, which decreased over time as indicated by decreasing sedimentation rates (Figure 5f) and increasing grain sizes (Figure 5b). The radiogenic Hf isotope signature was amplified by the prevailing fine-grained material dominated by labile minerals with highly radiogenic Hf isotope signatures (described in section 4.3.2.1).

4.3.2.1. The Evolution of Dissolved Hf in the Atlantic Sector of the Southern Ocean

Based on the results discussed above, we interpret more radiogenic Hf isotope ratios (ε_{Hf} above +5) in the Miocene and Pliocene (see Figure 5d) to be derived from partial dissolution of young volcanogenic particles of South American provenance. Although large contributions from this source are not evident in present-day seawater in the SO [*Stichel et al.*, 2012a; *Rickli et al.*, 2014], it is likely that different wind fields in the past (e.g., westerly wind field further poleward in the warmer Miocene and Pliocene [cf. *Toggweiler et al.*, 2006]) delivered larger amounts of South American sourced dust to the Agulhas Ridge. While in the modern SO Hf concentrations in seawater close to the Agulhas Ridge are extremely low, unradiogenic Nd isotope compositions show that terrigenous inputs from the Southern African continent are significant [*Stichel et al.*, 2012b]. This shows that inputs from an additional external source may have altered the seawater Hf isotope composition easily. Thus, it is likely that South American dust-derived Hf dominated the seawater signature when atmospheric import of dust from the west was enhanced and leads to more radiogenic Hf isotope ratios at the Agulhas Ridge without significantly affecting the detrital and dissolved Nd isotope compositions.

With the end of the Pliocene the influence of South American dust particles on dissolved Hf ceased and the predominance of (less radiogenic) Hf of Southern African origin was established. Although ice core and sedimentary records from Antarctica and the SO show that dust from South America was also exported to the region during the Pleistocene [e.g., *Basile et al.*, 1997; *Diekmann et al.*, 2000] and even strengthened during glacial episodes [*Lambert et al.*, 2008], it did not exert significant influence on the dissolved Hf in seawater above the Agulhas Ridge any more. These interpretations are in agreement with progressively increasing abundances of kaolinite minerals (from tropical and subtropical Africa; Figure 5c) mirroring the gradual strengthening of the Agulhas leakage until it stabilized in the latest Pliocene [*Diekmann et al.*, 2003]. Subsequently, the stronger Agulhas current largely prevented radiogenic Hf from partial dissolution of South American dust particles to reach the surface waters at the Agulhas Ridge.

Accordingly, the apparently parallel evolution of our Agulhas ridge seawater ε_{Hf} record and those of North Atlantic crusts ALV539 and BM1969 (Figure 5d) after 3 Ma is the result of the long-term evolution in particle provenance due to changes of atmospheric and oceanic circulation in the Southern Hemisphere. The similarity in the records does thus not reflect a causal relationship.

4.3.2.2. Tracing Inputs of Patagonian Dust in the Southern Ocean

Radiogenic peaks of 2–3 ε units in our seawater ε_{Hf} record at ~12 to 10.6 Ma and at ~7 Ma, as well as at 2.8 Ma in the late Pliocene reaching values above +8 were likely the result of highly incongruent dissolution of erosional products of the South American continent. Partial dissolution of the mostly volcanogenic dust likely acted as a significant source of highly radiogenic Hf given that other detrital inputs at the Agulhas Ridge have been very low. The isotopic composition of dust itself varied with atmospheric loading and likely amplified highly incongruent Hf isotope compositions (e.g., due to zircon loss during aeolian transport [*Rickli et al.*, 2010]).

Increased input and partial dissolution of dust particles from arid regions was demonstrated to be an important source of radiogenic Hf to the ocean as reflected by elevated Hf concentrations for surface waters west of the Sahara, which are up to 10 ε_{Hf} units more radiogenic than the bulk dust composition [*Rickli et al.*, 2010]. Consequently, the dominating westerly winds in the region that have delivered large amounts of South America sourced dust to the SO have contributed significantly to the oceanic Hf budget. Phases of increased dust deposition from South America were a consequence of past environmental conditions [e.g., *Sugden et al.*, 2009], which were probably also linked to the uplift of the Andean mountain range since the Miocene, which reached elevations severely altering South American climate between 4 and 3 Ma [e.g., *Hartley*, 2003].

5. Conclusions

1. Past mixing proportions between precursors of modern NADW and CDW/Pacific waters are reconstructed by using seawater Nd isotope compositions. An average of 69%$_{NCW}$ similar to modern SO water mass

mixing at the Agulhas ridge suggests that the general configuration of the circulation system has prevailed for the past 14 Myr, which was, however, interrupted by short-term perturbations throughout the entire investigated period of time.

2. The continuous evolution from highly radiogenic to less radiogenic Hf isotope signatures between 14 Ma and at the Pliocene indicates the gradual increase in the supply Hf originating from partial dissolution of particles from Southern Africa, which were transported by a stronger Agulhas current at the expense of South American sourced Hf, which prevailed during the Miocene and early Pliocene. Hf isotopes in the SO do not reflect variations due to glacial activity and subsequent changes of the AMOC.
3. We attribute Miocene/Pliocene excursions around 11 Ma, from 8 to 7 Ma, and near 2.8 Ma present in both Hf and Nd isotope signatures to phases of substantially decreased NCW admixture. Switches to more arid conditions in South America causing increased inputs of highly radiogenic Hf via aeolian dust occurred at a similar timing.
4. A period of early Pliocene warmth was accompanied by enhanced AMOC strength and NADW inflow into the Southern Ocean.
5. At 2.8 Ma, during MIS G10, the first large-scale glaciation in the Northern Hemisphere was accompanied by a pronounced weakening of the AMOC and a subsequent expansion of SCW, which was also notable in the North Atlantic.
6. A phase of stable and relatively strong AMOC between 2.5 and 1.5 Ma was finally followed by the late Pleistocene icehouse conditions, during which major glacial drops in NADW supply occurred. Analogously, increased glacial AMOC strength is evident in our records for roughly 200 kyr before the 900 ka transglacial event [*Pena and Goldstein*, 2014], which marked the transition to the modern mode of G-I oscillations in AMOC strength at the 100 kyr periodicity.
7. A comparison of ε_{Nd} values of intermediate waters from the Agulhas Ridge and the deep Cape and Agulhas Basin points to a less well-mixed SO during the last glacial. This is in agreement with recent findings of *Hu et al.* [2016].

Acknowledgments

All new data are available at https://doi.pangaea.de/10.1594/PANGAEA.871943. Sediment material for this study was provided by the ODP/IODP core repository in Bremen. Walter Hale and Alex Wülbers are thanked for their assistance during the sampling of ODP core 1088. We thank Tianyu Chen who helped to develop an appropriate leaching method for the sediment samples. Chris Siebert and Anne Osbourne are thanked for help with chemical separation and MC-ICP-MS measurements. We thank Jutta Heinze, Peer Rahlf, Ingmar Schindlbeck, and Julia Langer for help with sample preparation and assistance in the laboratory. We are grateful to Ellen Thomas and Christopher Reinhard for editorial handling. We acknowledge the comments from two anonymous reviewers that helped to improve the manuscript.

References

Abbott, A. N., B. A. Haley, and J. McManus (2015), Bottoms up: Sedimentary control of the deep North Pacific Ocean's ε_{Nd} signature, *Geology*, *43*(11), 1035–1038, doi:10.1130/G37114.1.

Abouchami, W., S. L. Goldstein, S. J. G. Gazer, A. Eisenhauer, and A. Mangini (1997), Secular changes of lead and neodymium in central Pacific seawater recorded by a Fe-Mn crust, *Geochim. Cosmochim. Acta*, *61*(18), 3957–3974, doi:10.1016/S0016-7037(97)00218-4.

Adkins, J. F. (2013), The role of deep ocean circulation in setting glacial climates, *Paleoceanography*, *28*, 539–561, doi:10.1002/palo.20046.

Albarède, F., A. Simonetti, J. D. Vervoort, J. Blichert-Toft, and W. Abouchami (1998), A Hf-Nd isotopic correlation in ferromanganese nodules, *Geophys. Res. Lett.*, *25*(20), 3895, doi:10.1029/1998GL900008.

Arsouze, T., J.-C. Dutay, F. Lacan, and C. Jeandel (2009), Reconstructing the Nd oceanic cycle using a coupled dynamical – biogeochemical model, *Biogeosci. Discuss.*, *6*(3), 5549–5588, doi:10.5194/bgd-6-5549-2009.

Balan, E., P. Trocellier, J. Jupille, E. Fritsch, J. P. Muller, and G. Calas (2001), Surface chemistry of weathered zircons, *Chem. Geol.*, *181*(1–4), 13–22, doi:10.1016/S0009-2541(01)00271-6.

Basile, I., F. E. Grousset, M. Revel, J. R. Petit, P. E. Biscaye, and N. I. Barkov (1997), Patagonian origin of glacial dust deposited in East Antarctica (Vostok and Dome C) during glacial stages 2, 4 and 6, *Earth Planet. Sci. Lett.*, *146*(3), 573–589, doi:10.1016/S0012-821X(96)00255-5.

Bassinot, F. C., L. D. Labeyrie, E. Vincent, X. Quidelleur, N. J. Shackleton, and Y. Lancelot (1994), The astronomical theory of climate and the age of the Brunhes-Matuyama magnetic reversal, *Earth Planet. Sci. Lett.*, *126*(1–3), 91–108, doi:10.1016/0012-821X(94)90244-5.

Bau, M., and A. Koschinsky (2006), Hafnium and neodymium isotopes in seawater and in ferromanganese crusts: The "element perspective.", *Earth Planet. Sci. Lett.*, *241*(3–4), 952–961, doi:10.1016/j.epsl.2005.09.067.

Bayon, G., N. Vigier, K. W. Burton, A. Brenot, J. Carignan, J. Etoubleau, and N. C. Chu (2006), The control of weathering processes on riverine and seawater hafnium isotope ratios, *Geology*, *34*(6), 433–436, doi:10.1130/G22130.1.

Bayon, G., K. W. Burton, G. Soulet, N. Vigier, B. Dennielou, J. Etoubleau, E. Ponzevera, C. R. German, and R. W. Nesbitt (2009), Hf and Nd isotopes in marine sediments: Constraints on global silicate weathering, *Earth Planet. Sci. Lett.*, *277*(3–4), 318–326, doi:10.1016/j.epsl.2008.10.028.

Bayon, G., C. Skonieczny, C. Delvigne, S. Toucanne, S. Bermell, E. Ponzevera, and L. André (2016), Environmental Hf–Nd isotopic decoupling in World river clays, *Earth Planet. Sci. Lett.*, *438*, 25–36, doi:10.1016/j.epsl.2016.01.010.

Biastoch, A., C. W. Böning, and J. R. E. Lutjeharms (2008), Agulhas leakage dynamics affects decadal variability in Atlantic overturning circulation, *Nature*, *456*(7221), 489–492, doi:10.1038/nature07426.

Billups, K. (2002), Late Miocene through early Pliocene deep water circulation and climate change viewed from the sub-Antarctic South Atlantic, *Palaeogeogr. Palaeoclimatol. Palaeoecol.*, *185*(3–4), 287–307, doi:10.1016/S0031-0182(02)00340-1.

Billups, K., C. Kelly, and E. Pierce (2008), The late Miocene to early Pliocene climate transition in the Southern Ocean, *Palaeogeogr. Palaeoclimatol. Palaeoecol.*, *267*(1–2), 31–40, doi:10.1016/j.palaeo.2008.05.013.

Blaser, P., J. Lippold, M. Gutjahr, N. Frank, J. M. Link, and M. Frank (2016), Extracting foraminiferal seawater Nd isotope signatures from bulk deep sea sediment by chemical leaching, *Chem. Geol.*, *439*, 189–204, doi:10.1016/j.chemgeo.2016.06.024.

Böhm, E., J. Lippold, M. Gutjahr, M. Frank, P. Blaser, B. Antz, J. Fohlmeister, N. Frank, M. B. Andersen, and M. Deininger (2015), Strong and deep Atlantic meridional overturning circulation during the last glacial cycle, *Nature*, *517*(7534), 73–76, doi:10.1038/nature14059.

Boyle, E. A., and L. D. Keigwin (1982), Deep circulation of the North Atlantic over the last 200,000 years: Geochemical evidence, *Science*, *218*(4574), 784–7, doi:10.1126/science.218.4574.784.
Broecker, W. S., D. M. Peteet, and D. Rind (1985), Does the ocean-atmosphere system have more than one stable mode of operation?, *Nature*, *315*(2), 21–26, doi:10.1038/315021a0.
Burton, K. W., D. C. Lee, J. N. Christensen, A. N. Halliday, and J. R. Hein (1999), Actual timing of neodymium isotopic variations recorded by Fe-Mn crusts in the western North Atlantic, *Earth Planet. Sci. Lett.*, *171*(1), 149–156, doi:10.1016/S0012-821X(99)00138-7.
Carter, P., D. Vance, C. D. Hillenbrand, J. A. Smith, and D. R. Shoosmith (2012), The neodymium isotopic composition of waters masses in the eastern Pacific sector of the Southern Ocean, *Geochim. Cosmochim. Acta*, *79*, 41–59, doi:10.1016/j.gca.2011.11.034.
Censarek, B., and R. Gersonde (2002), Miocene diatom biostratigraphy at ODP sites 689, 690, 1088, 1092 (Atlantic sector of the Southern Ocean), *Mar. Micropaleontol.*, *45*(3–4), 309–356, doi:10.1016/S0377-8398(02)00034-8.
Chen, T. Y., M. Frank, B. a. Haley, M. Gutjahr, and R. F. Spielhagen (2012), Variations of North Atlantic inflow to the central Arctic Ocean over the last 14 million years inferred from hafnium and neodymium isotopes, *Earth Planet. Sci. Lett.*, *353–354*, 82–92, doi:10.1016/j.epsl.2012.08.012.
Chen, T. Y., G. Li, M. Frank, and H. F. Ling (2013a), Hafnium isotope fractionation during continental weathering: Implications for the generation of the seawater Nd-Hf isotope relationships, *Geophys. Res. Lett.*, *40*, 916–920, doi:10.1002/grl.50217.
Chen, T. Y., R. Stumpf, M. Frank, J. Beldowski, and M. Staubwasser (2013b), Contrasting geochemical cycling of hafnium and neodymium in the central Baltic Sea, *Geochim. Cosmochim. Acta*, *123*, 166–180, doi:10.1016/j.gca.2013.09.011.
Curry, W. B., and G. P. Lohmann (1982), Carbon isotopic changes in benthic foraminifera from the western South Atlantic: Reconstruction of glacial abyssal circulation patterns, *Quatern. Res.*, *18*(2), 218–235, doi:10.1016/0033-5894(82)90071-0.
Dausmann, V., M. Frank, C. Siebert, M. Christl, and J. R. Hein (2015), The evolution of weathering inputs and deep ocean circulation in the Arctic Ocean since the Late Miocene: Radiogenic isotope evidence, *Earth Planet. Sci. Lett.*, *419*, 111–124, doi:10.1016/j.epsl.2015.03.007.
Diekmann, B., G. Kuhn, V. Rachold, A. Abelmann, U. Brathauer, D. K. Fütterer, R. Gersonde, and H. Grobe (2000), Terrigenous sediment supply in the Scotia Sea (Southern Ocean): Response to Late Quaternary ice dynamics in Patagonia and on the Antarctic Peninsula, *Palaeogeogr. Palaeoclimatol. Palaeoecol.*, *162*(3), 357–387, doi:10.1016/S0031-0182(00)00138-3.
Diekmann, B., M. Fälker, and G. Kuhn (2003), Environmental history of the south-eastern South Atlantic since the Middle Miocene: Evidence from the sedimentological records of ODP Sites 1088 and 1092, *Sedimentology*, *50*(3), 511–529, doi:10.1046/j.1365-3091.2003.00562.x.
Enfield, D. B., A. M. Mestas-Nuñez, and P. J. Trimble (2001), The Atlantic Multidecadal Oscillation and its relation to rainfall and river flows in the continental U.S, *Geophys. Res. Lett.*, *28*(10), 2077–2080, doi:10.1029/2000GL012745.
Ferrari, R., M. F. Jansen, J. F. Adkins, A. Burke, A. L. Stewart, and A. F. Thompson (2014), Antarctic sea ice control on ocean circulation in present and glacial climates, *Proc. Natl. Acad. Sci. U.S.A.*, *111*(24), 8753–8758, doi:10.1073/pnas.1323922111.
Filippova, A., M. Frank, M. Kienast, J. Rickli, E. Hathorne, I. M. Yashayaev, and P. Pahnke (2017), Water mass circulation and weathering inputs in the Labrador Sea based on coupled Hf–Nd isotope compositions and rare earth element distributions, *Geochim. Cosmochim. Acta*, *199*, 164–184, doi:10.1016/j.gca.2016.11.024.
Firdaus, M. L., T. Minami, K. Norisuye, and Y. Sohrin (2011), Strong elemental fractionation of Zr–Hf and Nb–Ta across the Pacific Ocean, *Nat. Geosci.*, *4*(4), 227–230, doi:10.1038/ngeo1114.
Frank, M. (2002), Radiogenic isotopes: Tracers of past ocean circulation and erosional input, *Rev. Geophys.*, *40*(1), 1001, doi:10.1029/2000RG000094.
Franzese, A. M., S. R. Hemming, S. L. Goldstein, and R. F. Anderson (2006), Reduced Agulhas Leakage during the Last Glacial Maximum inferred from an integrated provenance and flux study, *Earth Planet. Sci. Lett.*, *250*(1–2), 72–88, doi:10.1016/j.epsl.2006.07.002.
Gersonde, R., et al. (1999), Site 1088 Initial Report. *Proceedings of the Ocean Drilling Program*, *Initial Reports*, 177.
Godfrey, L. V., M. P. Field, and R. M. Sherrell (2008), Estuarine distributions of Zr, Hf, and Ag in the Hudson River and the implications for their continental and anthropogenic sources to seawater, *Geochem. Geophys. Geosyst.*, *9*, Q12007, doi:10.1029/2008GC002123.
Goldstein, S. L., and S. R. Hemming (2003), *Long-Lived Isotopic Tracers in Oceanography, Paleoceanography, and Ice-Sheet Dynamics*, Elsevier, Oxford.
Gordon, A. L., R. F. Weiss, W. M. Smethie, and M. J. Warner (1992), Thermocline and intermediate water communication between the south Atlantic and Indian oceans, *J. Geophys. Res.*, *97*(C5), 7223–7240, doi:10.1029/92JC00485.
Gutjahr, M., M. Frank, C. H. Stirling, V. Klemm, T. van de Flierdt, and A. N. Halliday (2007), Reliable extraction of a deepwater trace metal isotope signal from Fe-Mn oxyhydroxide coatings of marine sediments, *Chem. Geol.*, *242*(3–4), 351–370, doi:10.1016/j.chemgeo.2007.03.021.
Gutjahr, M., M. Frank, J. Lippold, and A. N. Halliday (2014), Peak last glacial weathering intensity on the North American continent recorded by the authigenic Hf isotope composition of North Atlantic deep-sea sediments, *Quat. Sci. Rev.*, *99*, 97–117, doi:10.1016/j.quascirev.2014.06.022.
Hartley, A. J. (2003), Andean uplift and climate change, *J. Geol. Soc. London*, *160*(1), 7–10, doi:10.1144/0016-764902-083.
Haug, G. H., and R. Tiedemann (1998), Effect of the formation of the Isthmus of Panama on Atlantic Ocean thermohaline circulation, *Nature*, *393*(6686), 673–676, doi:10.1038/31447.
Hegner, E., H. J. Dauelsberg, M. M. Rutgers Van Der Loeff, C. Jeandel, and H. J. W. De Baar (2007), Nd isotopic constraints on the origin of suspended particles in the Atlantic Sector of the Southern Ocean, *Geochem. Geophys. Geosyst.*, *8*, Q10008, doi:10.1029/2007GC001666.
Henry, L. G., L. G. Henry, J. F. Mcmanus, W. B. Curry, N. L. Roberts, A. M. Piotrowski, and L. D. Keigwin (2016), North Atlantic ocean circulation and abrupt climate change during the last glaciation, *Science*, *353*, 470–474, doi:10.1126/science.aaf5529.
Hodell, D. A., and K. Venz (1992), Toward a high-resolution stable isotopic reord of the Southern Ocean during the Pliocene-Pleistocene (4.8 to 0.8 Ma), in *Antarctic Research Series*, pp. 265–310, AGU, Washington, D. C.
Hodell, D. A., C. D. Charles, J. H. Curtis, P. G. Mortyn, U. S. Ninnemann, and K. A. Venz (2003a), Data report: Oxygen isotope stratigraphy of ODP Leg 177 Sites 1088, 1089, 1090, 1093, and 1094, in *Proceedings of the Ocean Drilling Program, Scientific Results*, vol. 177(October 2001), pp. 1–26, Ocean Drill. Program, College Station, Tex.
Hodell, D. A., K. A. Venz, C. D. Charles, and U. S. Ninnemann (2003b), Pleistocene vertical carbon isotope and carbonate gradients in the South Atlantic sector of the Southern Ocean, *Geochem. Geophys. Geosyst.*, *4*(1), 1004, doi:10.1029/2002GC000367.
Hu, R., T. L. Noble, A. M. Piotrowski, I. N. McCave, H. C. Bostock, and H. L. Neil (2016), Neodymium isotopic evidence for linked changes in Southeast Atlantic and Southwest Pacific circulation over the last 200 kyr, *Earth Planet. Sci. Lett.*, *455*, 106–114, doi:10.1016/j.epsl.2016.09.027.
Jaccard, S. L., C. T. Hayes, A. Martínez-García, D. A. Hodell, R. F. Anderson, D. M. Sigman, and G. H. Haug (2013), Two modes of change in Southern Ocean productivity over the past million years, *Science*, *339*(6126), 1419–23, doi:10.1126/science.1227545.
Jackson, L. C., K. A. Peterson, C. D. Roberts, and R. A. Wood (2016), Recent slowing of Atlantic overturning circulation as a recovery from earlier strengthening, *Nat. Geosci.*, *9*, 518–522, doi:10.1038/ngeo2715.

Jacobsen, S. B., and G. J. Wasserburg (1980), Sm-Nd isoopic evolution of chondrites, *Earth Planet. Sci. Lett.*, *50*(1), 139–155.
Jansen, E., T. Fronval, F. Rack, and J. E. T. Channell (2000), Pliocene-Pleistocene ice rafting history and cyclicity in the Nordic Seas during the last 3.5 Myr, *Paleoceanography*, *15*(6), 709–721, doi:10.1029/1999PA000435.
Jeandel, C., J. K. Bishop, and A. Zindler (1995), Exchange of neodymium and its isotopes between seawater and small and large particles in the Sargasso Sea, *Geochim. Cosmochim. Acta*, *59*(3), 535–547, doi:10.1016/0016-7037(94)00367-U.
Khélifi, N., and M. Frank (2014), A major change in North Atlantic deep water circulation during the Early Pleistocene transition 1.6 million years ago, *Climate Past Discuss.*, *9*(6), 6495–6513, doi:10.5194/cpd-9-6495-2013.
Knies, J., et al. (2014), Effect of early Pliocene uplift on late Pliocene cooling in the Arctic-Atlantic gateway, *Earth Planet. Sci. Lett.*, *387*, 132–144, doi:10.1016/j.epsl.2013.11.007.
Lacan, F., and C. Jeandel (2005), Neodymium isotopes as a new tool for quantifying exchange fluxes at the continent-ocean interface, *Earth Planet. Sci. Lett.*, *232*(3–4), 245–257, doi:10.1016/j.epsl.2005.01.004.
Lambert, F., B. Delmonte, J. R. Petit, M. Bigler, P. R. Kaufmann, M. A. Hutterli, T. F. Stocker, U. Ruth, J. P. Steffensen, and V. Maggi (2008), Dust-climate couplings over the past 800,000 years from the EPICA Dome C ice core, *Nature*, *452*(7187), 616–619, doi:10.1038/nature06763.
Lang, D. C., et al. (2014), The transition on North America from the warm humid Pliocene to the glaciated Quaternary traced by eolian dust deposition at a benchmark North Atlantic Ocean drill site, *Quat. Sci. Rev.*, *93*, 125–141, doi:10.1016/j.quascirev.2014.04.005.
Lang, D. C., I. Bailey, P. A. Wilson, T. B. Chalk, G. L. Foster, and M. Gutjahr (2016), Incursions of southern-sourced water into the deep North Atlantic during late Pliocene glacial intensification, *Nat. Geosci.*, *9*, 375–379, doi:10.1038/ngeo2688.
Ling, H. F., K. W. Burton, R. K. O'Nions, B. S. Kamber, F. von Blanckenburg, A. J. Gibb, and J. R. Hein (1997), Evolution of Nd and Pb isotopes in Central Pacific seawater from ferromanganese crusts, *Earth Planet. Sci. Lett.*, *146*(1–2), 1–12, doi:10.1016/S0012-821X(96)00224-5.
Lippold, J., Y. Luo, R. Francois, S. E. Allen, J. Gherardi, S. Pichat, B. Hickey, and H. Schulz (2012), Strength and geometry of the glacial Atlantic Meridional Overturning Circulation, *Nat. Geosci.*, *5*(11), 813–816, doi:10.1038/ngeo1608.
Lisiecki, L. E., and M. E. Raymo (2005), A Pliocene-Pleistocene stack of 57 globally distributed benthic $\delta^{18}O$ records, *Paleoceanography*, *20*, PA1003, doi:10.1029/2004PA001071.
Lynch-Stieglitz, J., et al. (2007), Atlantic meridional overturning circulation during the Last Glacial Maximum, *Science*, *316*(5821), 66–69, doi:10.1126/science.1137127.
Marino, M., and J. A. Flores (2002), Miocene to Pliocene calcareous nannofossil biostratigraphy at ODP Leg 177 Sites 1088 and 1090, *Mar. Micropaleontol.*, *45*(3–4), 291–307, doi:10.1016/S0377-8398(02)00033-6.
Martin, J. H. (1990), Glacial-interglacial CO2 changes: The iron hypothesis, *Paleoceanography*, *5*(1), 1–13, doi:10.1029/PA005i001p00001.
Martínez-Botí, M. A., G. L. Foster, T. B. Chalk, E. J. Rohling, P. F. Sexton, D. J. Lunt, R. D. Pancost, M. P. S. Badger, and D. N. Schmidt (2015), Plio-Pleistocene climate sensitivity evaluated using high-resolution CO_2 records, *Nature*, *518*(7537), 49–54, doi:10.1038/nature14145.
McManus, J. F., R. Francois, J.-M. Gherardi, L. D. Keigwin, and S. Brown-Leger (2004), Collapse and rapid resumption of Atlantic meridional circulation linked to deglacial climate changes, *Nature*, *428*(6985), 834–837, doi:10.1038/nature02494.
Miller, K. G., G. S. Mountain, J. V. Browning, M. Kominz, P. J. Sugarman, N. Christie-Blick, M. E. Katz, and J. D. Wright (1998), Cenozoic global sea level, sequences, and the New Jersey Transect: Results from coastal plain and continental slope drilling, *Rev. Geophys.*, *36*(4), 569–601, doi:10.1029/98RG01624.
Mix, A. C., N. G. Pisias, W. Rugh, J. Wilson, A. Morey, and T. K. Hagelberg (1995), Benthic foraminifer stable isotope record from Site 849 (0–5 Ma): Local and global climate changes, *Proc. Ocean Drill. Program Sci. Results*, *138*, 371–412.
Münker, C., S. Weyer, E. Scherer, and K. Mezger (2001), Separation of high field strength elements (Nb, Ta, Zr, Hf) and Lu from rock samples for MC-ICPMS measurements, *Geochem. Geophys. Geosyst.*, *1*(12), doi:10.1029/2001GC000183.
Noble, T. L., A. M. Piotrowski, L. F. Robinson, J. F. McManus, C. D. Hillenbrand, and A. J. M. Bory (2012), Greater supply of Patagonian-sourced detritus and transport by the ACC to the Atlantic sector of the Southern Ocean during the last glacial period, *Earth Planet. Sci. Lett.*, *317–318*, 374–385, doi:10.1016/j.epsl.2011.10.007.
Nowell, G. M., P. D. Kempton, S. R. Noble, A. D. Saunders, J. J. Mahoney, and R. N. Taylor (1998), High-precision Hf isotopic measurements of MORB and OIB by thermal ionization mass-spectrometry: insights into the depleted mantle, *Chem. Geol.*, *149*(3), 211–233.
O'Nions, R., M. Frank, F. von Blanckenburg, and H.-F. Ling (1998), Secular variation of Nd and Pb isotopes in ferromanganese crusts from the Atlantic, Indian and Pacific Oceans, *Earth Planet. Sci. Lett.*, *155*(1–2), 15–28, doi:10.1016/S0012-821X(97)00207-0.
Oppo, D. W., and R. G. Fairbanks (1987), Variability in the deep and intermediate water circulation of the Atlantic Ocean during the past 25,000 years: Northern Hemisphere modulation of the Southern Ocean, *Earth Planet. Sci. Lett.*, *86*(1), 1–15, doi:10.1016/0012-821X(87)90183-X.
Orsi, A. H., T. Whitworth, and W. D. Nowlin (1995), On the meridional extent and fronts of the Antarctic Circumpolar Current, *Deep-Sea Res. I Oceanogr. Res. Pap.*, *42*(5), 641–673, doi:10.1016/0967-0637(95)00021-W.
Pena, L. D., and S. L. Goldstein (2014), Thermohaline circulation crisis and impacts during the mid-Pleistocene transition, *Science*, *345*(6194), 318–322, doi:10.1126/science.1249770.
Petschick, R., G. Kuhn, and F. Gingele (1996), Clay mineral distribution in surface sediments of the South Atlantic: Sources, transport, and relation to oceanography, *Mar. Geol.*, *130*(3–4), 203–229, doi:10.1016/0025-3227(95)00148-4.
Piepgras, D., and G. Wasserburg (1982), Isotopic composition of neodymium in waters from the Drake Passage, *Science*, *217*(4556), 207–214, doi:10.1126/science.217.4556.207.
Pin, C., and J. F. S. Zalduegui (1997), Sequential separation of light rare-earth elements, thorium and uranium by miniaturized extraction chromatography: Application to isotopic analyses of silicate rocks, *Anal. Chim. Acta*, *339*(1–2), 79–89, doi:10.1016/S0003-2670(96)00499-0.
Piotrowski, A. M. (2005), Temporal relationships of carbon cycling and ocean circulation at glacial boundaries, *Science*, *307*(5717), 1933–1938, doi:10.1126/science.1104883.
Piotrowski, A. M., D.-C. Lee, J. N. Christensen, K. W. Burton, A. N. Halliday, J. R. Hein, and D. Günther (2000), Changes in erosion and ocean circulation recorded in the Hf isotopic compositions of North Atlantic and Indian Ocean ferromanganese crusts, *Earth Planet. Sci. Lett.*, *181*(3), 315–325, doi:10.1016/S0012-821X(00)00205-3.
Piotrowski, A. M., S. L. Goldstein, S. R. Hemming, and R. G. Fairbanks (2004), Intensification and variability of ocean thermohaline circulation through the last deglaciation, *Earth Planet. Sci. Lett.*, *225*(1–2), 205–220, doi:10.1016/j.epsl.2004.06.002.
Piotrowski, A. M., S. L. Goldstein, S. R. Hemming, R. G. Fairbanks, and D. R. Zylberberg (2008), Oscillating glacial northern and southern deep water formation from combined neodymium and carbon isotopes, *Earth Planet. Sci. Lett.*, *272*(1–2), 394–405, doi:10.1016/j.epsl.2008.05.011.
Piotrowski, A. M., V. K. Banakar, A. E. Scrivner, H. Elderfield, A. Galy, and A. Dennis (2009), Indian Ocean circulation and productivity during the last glacial cycle, *Earth Planet. Sci. Lett.*, *285*(1–2), 179–189, doi:10.1016/j.epsl.2009.06.007.
Raymo, M. (1994), The initiation of Northern Hemisphere Glaciation, *Annu. Rev. Earth Planet. Sci.*, *22*(1), 353–383, doi:10.1146/annurev.earth.22.1.353.

Raymo, M. E., W. F. Ruddiman, N. J. Shackleton, and D. W. Oppo (1990), Evolution of Atlantic-Pacific d^{13}C gradients over the last 2.5 m.y, *Earth Planet. Sci. Lett.*, *97*(3–4), 353–368, doi:10.1016/0012-821X(90)90051-X.

Raymo, M. E., B. Grant, M. Horowitz, and G. H. Rau (1996), Mid-Pliocene warmth: Stronger greenhouse and stronger conveyor, *Mar. Micropaleontol.*, *27*(1–4), 313–326, doi:10.1016/0377-8398(95)00048-8.

Reid, J. (1996), On the circulation of the South Atlantic Ocean, in *The South Atlantic*, pp. 13–44, Springer Berlin Heidelberg, Berlin, Heidelberg.

Rempfer, J., T. F. Stocker, F. Joos, J. C. Dutay, and M. Siddall (2011), Modelling Nd-isotopes with a coarse resolution ocean circulation model: Sensitivities to model parameters and source/sink distributions, *Geochim. Cosmochim. Acta*, *75*(20), 5927–5950, doi:10.1016/j.gca.2011.07.044.

Rempfer, J., T. F. Stocker, F. Joos, and J.-C. Dutay (2012), Sensitivity of Nd isotopic composition in seawater to changes in Nd sources and paleoceanographic implications, *J. Geophys. Res.*, *117*, C12010, doi:10.1029/2012JC008161.

Rickli, J., M. Frank, and A. N. Halliday (2009), The hafnium-neodymium isotopic composition of Atlantic seawater, *Earth Planet. Sci. Lett.*, *280*(1–4), 118–127, doi:10.1016/j.epsl.2009.01.026.

Rickli, J., M. Frank, A. R. Baker, S. Aciego, G. de Souza, R. B. Georg, and A. N. Halliday (2010), Hafnium and neodymium isotopes in surface waters of the eastern Atlantic Ocean: Implications for sources and inputs of trace metals to the ocean, *Geochim. Cosmochim. Acta*, *74*(2), 540–557, doi:10.1016/j.gca.2009.10.006.

Rickli, J., M. Gutjahr, D. Vance, M. Fischer-Gödde, C. D. Hillenbrand, and G. Kuhn (2014), Neodymium and hafnium boundary contributions to seawater along the West Antarctic continental margin, *Earth Planet. Sci. Lett.*, *394*, 99–110, doi:10.1016/j.epsl.2014.03.008.

Roberts, N. L., and A. M. Piotrowski (2015), Radiogenic Nd isotope labeling of the northern NE Atlantic during MIS 2, *Earth Planet. Sci. Lett.*, *423*, 125–133, doi:10.1016/j.epsl.2015.05.011.

Robson, J., P. Ortega, and R. Sutton (2015), A recent reversal of climatic trends in the North Atlantic, *Nat. Geosci.*, *9*(June), 1–15, doi:10.1038/ngeo2727.

Rutberg, R., S. Hemming, and S. Goldstein (2000), Reduced North Atlantic Deep Water flux to the glacial Southern Ocean inferred from neodymium isotope ratios, *Nature*, *405*(6789), 935–8, doi:10.1038/35016049.

Scher, H. D., and E. E. Martin (2004), Circulation in the Southern Ocean during the Paleogene inferred from neodymium isotopes, *Earth Planet. Sci. Lett.*, *228*(3–4), 391–405, doi:10.1016/j.epsl.2004.10.016.

Scher, H. D., and E. E. Martin (2008), Oligocene deep water export from the North Atlantic and the development of the Antarctic Circumpolar Current examined with neodymium isotopes, *Paleoceanography*, *23*, PA1205, doi:10.1029/2006PA001400.

Siddall, M., S. Khatiwala, T. van de Flierdt, K. Jones, S. L. Goldstein, S. Hemming, and R. F. Anderson (2008), Towards explaining the Nd paradox using reversible scavenging in an ocean general circulation model, *Earth Planet. Sci. Lett.*, *274*(3–4), 448–461, doi:10.1016/j.epsl.2008.07.044.

Skinner, L. C., A. E. Scrivner, D. Vance, S. Barker, S. Fallon, and C. Waelbroeck (2013), North atlantic versus Southern Ocean contributions to a deglacial surge in deep ocean ventilation, *Geology*, *41*(6), 667–670, doi:10.1130/G34133.1.

Stichel, T., M. Frank, J. Rickli, and B. a. Haley (2012a), The hafnium and neodymium isotope composition of seawater in the Atlantic sector of the Southern Ocean, *Earth Planet. Sci. Lett.*, *317–318*, 282–294, doi:10.1016/j.epsl.2011.11.025.

Stichel, T., M. Frank, J. Rickli, E. C. Hathorne, B. a. Haley, C. Jeandel, and C. Pradoux (2012b), Sources and input mechanisms of hafnium and neodymium in surface waters of the Atlantic sector of the Southern Ocean, *Geochim. Cosmochim. Acta*, *94*, 22–37, doi:10.1016/j.gca.2012.07.005.

Sugden, D. E., R. D. McCulloch, A. J.-M. Bory, and A. S. Hein (2009), Influence of Patagonian glaciers on Antarctic dust deposition during the last glacial period, *Nat. Geosci.*, *2*(4), 281–285, doi:10.1038/ngeo474.

Sutton, R. T., and D. L. R. Hodson (2005), Atlantic Ocean forcing of North American and European summer climate, *Science*, *309*(5731), 115–8, doi:10.1126/science.1109496.

Tachikawa, K. (2003), Neodymium budget in the modern ocean and paleo-oceanographic implications, *J. Geophys. Res.*, *108*(C8), 3254, doi:10.1029/1999JC000285.

Tanaka, T., et al. (2000), JNdi-1: A neodymium isotopic reference in consistency with LaJolla neodymium, *Chem. Geol.*, *168*(3–4), 279–281, doi:10.1016/S0009-2541(00)00198-4.

Toggweiler, J. R., J. L. Russell, and S. R. Carson (2006), Midlatitude westerlies, atmospheric CO_2, and climate change during the ice ages, *Paleoceanography*, *21*, PA2005, doi:10.1029/2005PA001154.

Uenzelmann-Neben, G., and K. Gohl (2004), The Agulhas Ridge, South Atlantic: The peculiar structure of a fracture zone, *Mar. Geophys. Res.*, *25*(3–4), 305–319, doi:10.1007/s11001-005-1338-8.

van de Flierdt, T., M. Frank, D. C. Lee, and A. N. Halliday (2002), Glacial weathering and the hafnium isotope composition of seawater, *Earth Planet. Sci. Lett.*, *201*(3–4), 639–647, doi:10.1016/S0012-821X(02)00731-8.

van de Flierdt, T., S. L. Goldstein, S. R. Hemming, M. Roy, M. Frank, and A. N. Halliday (2007), Global neodymium-hafnium isotope systematics—Revisited, *Earth Planet. Sci. Lett.*, *259*(3–4), 432–441, doi:10.1016/j.epsl.2007.05.003.

Venz, K. A., and D. A. Hodell (2002), New evidence for changes in Plio–Pleistocene deep water circulation from Southern Ocean ODP Leg 177 Site 1090, *Palaeogeogr. Palaeoclimatol. Palaeoecol.*, *182*(3–4), 197–220, doi:10.1016/S0031-0182(01)00496-5.

Vervoort, J. D., P. J. Patchett, J. Blichert-Toft, and F. Albarède (1999), Relationships between Lu-Hf and Sm-Nd isotopic systems in the global sedimentary system, *Earth Planet. Sci. Lett.*, *168*(1–2), 79–99, doi:10.1016/S0012-821X(99)00047-3.

Vervoort, J. D., T. Plank, and J. Prytulak (2011), The Hf-Nd isotopic composition of marine sediments, *Geochim. Cosmochim. Acta*, *75*(20), 5903–5926, doi:10.1016/j.gca.2011.07.046.

Walter, H. J., E. Hegner, B. Diekmann, G. Kuhn, and M. M. Rutgers Van Der Loeff (2000), Provenance and transport of terrigenous sediment in the South Atlantic Ocean and their relations to glacial and interglacial cycles: Nd and Sr isotopic evidence, *Geochim. Cosmochim. Acta*, *64*(22), 3813–3827, doi:10.1016/S0016-7037(00)00476-2.

White, W. M., J. Patchett, and D. BenOthman (1986), Hf isotope ratios of marine sediments and Mn nodules: Evidence for a mantle source of Hf in seawater, *Earth Planet. Sci. Lett.*, *79*(1–2), 46–54, doi:10.1016/0012-821X(86)90039-7.

Wilson, D. J., A. M. Piotrowski, A. Galy, and J. a. Clegg (2013), Reactivity of neodymium carriers in deep sea sediments: Implications for boundary exchange and paleoceanography, *Geochim. Cosmochim. Acta*, *109*, 197–221, doi:10.1016/j.gca.2013.01.042.

Yu, J., et al. (2016), Sequestration of carbon in the deep Atlantic during the last glaciation, *Nat. Geosci.*, *9*(4), 319–324, doi:10.1038/ngeo2657.